

# **An alternatively translated isoform of *PPARG* proposes AF-1 domain inhibition as an insulin sensitization target**

Truncated PPAR $\gamma$  may be insulin sensitizing

Xiaomi Du<sup>1,2</sup>, Karen Mendez-Lara<sup>1</sup>, Siqi Hu<sup>1</sup>, Rachel Diao<sup>1</sup>, Guru Bhavimani<sup>1</sup>, Ruben Hernandez<sup>1</sup>, Kimberly Glass<sup>1</sup>, Camila De Arruda Saldanha<sup>1</sup>, Jason Flannick<sup>3,4</sup>, Sven Heinz<sup>1</sup>,  
Amit R. Majithia<sup>1a</sup>

<sup>1</sup> Division of Endocrinology and Metabolism, Department of Medicine, University of California, San Diego, La Jolla, CA, USA

<sup>2</sup> Bioinformatics and Systems Biology Graduate Program, University of California, San Diego, La Jolla, CA, USA

<sup>3</sup> Program in Medical and Population Genetics, Broad Institute of MIT and Harvard, Cambridge, MA, USA

<sup>4</sup> Department of Pediatrics, Boston Children's Hospital, Boston, MA, USA

<sup>a</sup> To whom correspondence should be addressed.

T: (858)-822-0727

E: [amajithia@ucsd.edu](mailto:amajithia@ucsd.edu)

Keywords: PPAR $\gamma$ , insulin sensitivity, metabolic syndrome, genetic screens, human genomics

Word count: 4,776

Number of main tables and figures: 5

## Abstract

PPAR $\gamma$  is the pharmacological target of thiazolidinediones (TZDs), potent insulin sensitizers that prevent metabolic disease morbidity but are accompanied by side effects such as weight gain, in part due to non-physiological transcriptional agonism. Using high throughput genome engineering, we targeted nonsense mutations to every exon of *PPARG*, finding an ATG in Exon 2 (chr3:12381414, CCDS2609 c.A403) that functions as an alternative translational start site. This downstream translation initiation site gives rise to a PPAR $\gamma$  protein isoform (M135), preferentially generated from alleles containing nonsense mutations upstream of c.A403. PPAR $\gamma$  M135 retains the DNA and ligand binding domains of full-length PPAR $\gamma$  but lacks the N-terminal AF-1 domain. Despite being truncated, PPAR $\gamma$  M135 shows increased transactivation of target genes, but only in the presence of agonists. Accordingly, human missense mutations disrupting AF-1 domain function actually increase agonist-induced cellular PPAR $\gamma$  activity compared to wild-type (WT), and carriers of these AF-1 disrupting variants are protected from metabolic syndrome. Thus, we propose the existence of PPAR $\gamma$  M135 as a fully functional, alternatively translated isoform that may be therapeutically generated to treat insulin resistance-related disorders.

## Article Highlights

- Genetic screens were performed across *PPARG* to study how disruptive mutations across the full coding sequence affect function.
- An alternative translational start site in *PPARG* generates a truncated isoform, PPAR $\gamma$  M135, which lacks the N-terminal AF-1 domain and shows increased agonist-induced transactivation of target genes.

- In human carriers of rare *PPARG* variants, AF-1 domain disrupting genetic variants increase agonist-induced PPAR $\gamma$  activity and decrease metabolic syndrome severity.
- Targeting the AF-1 domain is a potential therapeutic strategy for insulin sensitization.

## Introduction

Insulin resistance is a major driver of the epidemic metabolic diseases that challenge global health(1). Thiazolidinediones (TZDs) are a class of drugs that decrease insulin resistance by agonizing PPAR $\gamma$ (2), a nuclear hormone receptor that contains an autonomous activation-function domain 1 (AF-1), DNA binding domain (DBD), and ligand binding domain (LBD) (Figure 1A)(3). TZDs have demonstrated clinical efficacy in treating type 2 diabetes and cardiovascular disease (4), but their use has been limited by serious side effects, including weight gain and fluid retention(2). Much pharmacological development has been focused on the development of selective PPAR $\gamma$  modulators (SPPARMs) that retain the benefits of TZDs without the attendant adverse effects, but successful compounds have not reached the clinic(5). Thus, the need for alternative approaches to therapeutically activate PPAR $\gamma$  without PPAR-mediated side effects remains unmet.

Loss-of-function (LOF) mutations in *PPARG* occurring in the DBD and LBD have been shown to cause familial partial lipodystrophy type 3 (FPLD3), a Mendelian genetic syndrome characterized by insulin resistance, metabolic syndrome, and gluteofemoral fat loss(6,7). These pathogenic FPLD3 mutations establish the clinical significance of the PPAR $\gamma$  DBD and LBD, but they are only the tip of the iceberg in human protein-coding variants found in *PPARG*(8). In previous work, we have identified hundreds of protein-coding variants in *PPARG* occurring in all protein domains, including the AF-1 domain(9). As with FPLD3, those that cause LOF in the DBD

and LBD increase insulin resistance and type 2 diabetes risk. We observed no apparent clinical impact of LOF variants in the AF-1 domain, leaving in question its function in human metabolic health.

In this study, we report a novel protein isoform of PPAR $\gamma$  (named PPAR $\gamma$  M135), which lacks the AF-1 domain and is generated from an alternative translational start site. Through biochemical and transcriptomic profiling, we find that PPAR $\gamma$  M135 demonstrates enhanced ligand-inducible transcriptional and functional activity compared to WT, leading us to a model of de-repression by loss of AF-1. To evaluate the clinical consequence of this model, we identified and analyzed human carriers of *PPARG* variants that impair AF-1 function, finding that these variants increase PPAR $\gamma$  function and decrease metabolic syndrome severity in people who carry them. Taken together, our study nominates AF-1 domain inhibition as a new targetable mechanism to activate PPAR $\gamma$ .

## Research Design and Methods

### Cell Lines

Human monocytic leukemia cells (THP-1, ATCC #TIB-202) and human preadipocyte cells (Simpson-Golabi-Behmel Syndrome (SGBS)) were cultured, differentiated, and stimulated to activate PPAR $\gamma$  as described in **Supplementary Methods**. Statistical analysis did not include sex, as all cells originated from the same male cell lines.

### Pooled screens

Guide RNAs (sgRNAs) to target *PPARG* (Table S1) were cloned into lentiCRISPRv2 (Addgene #52961), and the vectors were pooled for virus production (Mirus Bio #2304). THP-1 cells were infected at MOI=0.3, and edited cells were selected for using puromycin (Sigma-Aldrich, #P8833).

To assess the functional impact of *PPARG* indels, cells were differentiated, stimulated, and FACS sorted based on CD36 expression (n=5 independent sorts). Enrichment scores (ES) were calculated as the log<sub>2</sub>-ratio of CD36<sup>+</sup>/CD36<sup>-</sup> normalized counts. The impact of indels at each codon of *PPARG* was calculated based on previously published methods (9).

### ***PPARG* edited cell lines**

The endonuclease Cas9 and guides Int-sgRNA, Ex1-sgRNA, Ex1-sgRNA2, and Ex3-sgRNA (Table S3) were introduced into THP-1 and SGBS cells by lentiviral transduction. The transduced THP-1 cells were sorted one cell per well into 96-well plates (BD FACSAria II) and expanded. Infected SGBS cells were differentiated 7 days after infection as previously published (10). Genomic edits and zygosity were confirmed by Sanger sequencing.

### **Western blotting**

Proteins were extracted, quantified, loaded into 4-12% Bis-Tris Gels (Invitrogen, NP0336), and transferred onto 0.45 um nitrocellulose membranes (Bio-Rad, #1620115). Antibodies used were Cell Signaling Technology (CST) #2435 (PPAR $\gamma$  N-terminus), CST #2443 (PPAR $\gamma$  C-terminus), CST #43603 (cyclophilin B (PPIB)), CST #41185 (actin), CST #2920 (Akt), CST #4060 (phospho-Akt Ser473), and fluorescent secondary antibodies CST #5366, #5151, and #5470. Imaging was performed on the Odyssey CLx imager (LI-COR).

### **THP-1 cells with exogenous PPAR $\gamma$**

To evaluate the complementation of PPAR $\gamma$  using wildtype (WT) and M135 PPAR $\gamma$  isoforms, in vitro transcription (IVT) was performed as previously described (11) with the following primers:

WT-FWD: 5'-  
 GAATTTAATACGACTCACTATAAGGAAATACGCCACCATGGGTGAAACTCTGGGAG  
 AT-3'; M135-FWD: 5'-

GAATTTAATACGACTCACTATAAGGAAATACGCCACCATGGCAATTGAATGTCGTGT  
 CT-3', and REV: 5'-  
 CTAGGACATCGCAGTCTGCACCTAGTACAAGTCCTTGTAGATCTCCTG-3'.

The transcripts were electroporated into  $P\gamma^{-/-}$  THP-1 cells in a 4 mm cuvette with one 400 V, 5 ms square wave pulse (BioRad XCell). To match PPAR $\gamma$  protein expression, 2  $\mu$ g of M135 mRNA and 8  $\mu$ g of WT mRNA were used for each electroporation of 3 million cells (n=5). Each sample was split into 3 aliquots for protein collection and differentiation  $-/+$  rosiglitazone treatment. RNA was extracted (Zymo #R1050) and sent for library preparation (Illumina Stranded mRNA Prep) and 100 bp paired-end sequencing (25 million reads/sample on the NovaSeq S4). Analysis was performed in R 4.1.3 using edgeR 3.36.0, limma v3.50.1, UpSetR v1.4.0, and fgsea v1.20.0 (12–15).

### **SGBS cells with exogenous PPAR $\gamma$**

*PPARG* cDNA was synthesized (Twist Bioscience) with synonymous mutations (CCDS2609 c.C594T, G603C, T610A, C511G) to eliminate the Ex3-sgRNA recognition sequence and PCR amplified to generate cDNA encoding PPAR $\gamma$ 2 and PPAR $\gamma$  M135. These sequences were cloned into doxycycline-inducible pCW (Addgene #184708). Virus was produced, and SGBS  $P\gamma^{-/-}$  cells were infected to create the SGBS  $P\gamma^{-/-}$  +WT and SGBS  $P\gamma^{-/-}$  +M135 cell lines. Insulin stimulation was performed after a 24 hour serum starvation with 100 nM insulin (Sigma Aldrich #I9278).

### **Human genetics**

For all exome sequenced cohorts, variants within the genomic coordinates of *PPARG* (chr3: 12287368-12434356 hg38) were extracted, and variant annotation was performed using SnpEff v4.3 (16). Nomenclature used for missense variants is for the canonical *PPARG* transcript ENST00000287820.10; protein ENSP00000287820.6. Function scores were obtained from the

*PPARG* saturation mutagenesis(9). Serum HDL cholesterol (field 30760), waist circumference (field 48), serum triglycerides (TG, field 30870), systolic blood pressure (SBP, field 4080), and glycated hemoglobin (HbA1c, field 30750), were extracted for all UK Biobank (UKB) participants. SBP values were corrected for individuals reported to be taking blood pressure medication by adding 15 mm Hg (17), and TG values were log-normalized. The TG/HDL ratio was log-transformed and z-normalized across the UKB. Regressions were adjusted for the covariates of age, age<sup>2</sup>, sex, and the first ten principal components of genetic ancestry.

### **Data and Resource Availability**

All biobank data used in this study are accessible through applications to the respective databases. Data and resources are available upon request to the corresponding author.

## **Results**

### **A novel functional PPAR $\gamma$ isoform, M135, is generated from an alternative translational start site**

In our initial experiments the endogenous *PPARG* locus was systematically disrupted by inducing insertions and deletions (indels) in each coding *PPARG* exon in a human macrophage cell line (THP-1), a tractable model suitable for large scale genetic perturbation that phenocopy *PPARG* related transcriptional responses in adipocytes(9,18). Findings from THP-1s were confirmed and extended in human adipocytes models, the physiologically relevant cell type for metabolic disease. The effect of *PPARG* disruptions was measured by quantifying the ability of the resulting cells to transactivate CD36, a direct PPAR $\gamma$  transcriptional target (19). A custom lentiviral library of CRISPR/Cas9 constructs with guides (sgRNAs) targeting all coding exons, untranslated regions, and introns (n=95, Table S1), was introduced into THP-1 monocytes at one

construct per cell. The resulting population of genome-edited cells was differentiated into macrophages, stimulated with 1  $\mu$ M PPAR $\gamma$  agonist rosiglitazone, and sorted by FACS according to the expression of CD36 (Figure 1B). The CD36<sup>+</sup> and CD36<sup>-</sup> populations were sequenced to recover the identities of the sgRNAs, and an enrichment score (ES) was calculated based on the counts of each sgRNA in the CD36<sup>+</sup>/CD36<sup>-</sup> pools (Figure 1B). Intron targeting sgRNAs introduced as controls had ES=0.487 $\pm$ 0.025. As expected, targeting sgRNAs to Exon B of *PPARG*, specific to the PPAR $\gamma$ 2 isoform, did not reduce CD36 activity (ES=0.622 $\pm$ 0.035), and most sgRNAs targeted to exons downstream of the PPAR $\gamma$ 1 start site caused severe loss of CD36 transactivation (ES=-1.33 $\pm$ 0.147). Intriguingly, five sgRNAs targeting Exon 1 of *PPARG*, downstream of the PPAR $\gamma$ 1 start site, which would be predicted to maximally disrupt the protein sequence, had little effect on CD36 transactivation (ES=0.597 $\pm$ 0.084), suggesting an intact PPAR $\gamma$  response in the cells that harbored them (Figure 1C).

To further understand this unexpected finding, we analyzed data generated from a previously conducted saturation mutagenesis study of *PPARG* that contained indels at every codon of the PPAR $\gamma$ 2 cDNA (CCDS2609) and calculated function scores (FS) such that wild-type *PPARG* has FS=0 (Table S2)(9). Most indels that caused frameshift terminations in *PPARG* completely inhibited CD36 transactivation, as shown by negative FS. However, frameshifting indels in the 5' region of the cDNA, predicted to cause early termination of protein translation, paradoxically retained cellular PPAR $\gamma$  transactivation (FS=0.0322 $\pm$ 0.0186). This concurred with our finding of tolerated Exon 1 disruptions at the endogenous *PPARG* locus (Figure 1C) and suggested a possible post-splicing mechanism for retained PPAR $\gamma$  activity. The tolerance to early frameshifting indels was observed until c.A403, after which frameshifting indels induced significant dysfunction (FS=-1.16 $\pm$ 0.0074). These findings were replicated in experiments using

prostaglandin J2, a putatively endogenous PPAR $\gamma$  ligand(9) (Figure S1A). C.A403-405 encodes a methionine, leading us to hypothesize an alternative translation initiation site, which would explain the preservation of PPAR $\gamma$  transactivation functions in transcripts with frameshift and nonsense-inducing indels prior to c.A403.

A translation initiation site at CCDS2609 c.A403 (hg38:chr3:12381414; ENSP00000287820 p.M135) would lead to a protein isoform (PPAR $\gamma$  M135) shorter than PPAR $\gamma$ 2 by 134 amino acids with a predicted molecular weight of ~40 kDa. To evaluate this hypothesis, we engineered clonal THP-1 monocytes with disruptions in Exon 1, Exon 3, and a *PPARG* intron using CRISPR/Cas9 (Ex1-sgRNA chr3:12379745, Ex3-sgRNA chr3:12392733, Int-sgRNA chr3:12363492, Figure 1A). Two independent cell lines were derived for each of the following genotypes: Int-sgRNA +/+, Ex1-sgRNA +/-, Ex1-sgRNA -/-, and Ex3-sgRNA -/- (Table S3). Immunoblotting with PPAR $\gamma$  antibodies targeting N-terminal (p.Asp69) and C-terminal (p.His494) epitopes was performed on differentiated THP-1s. The N-terminal blot showed a 53 kDa band for full-length PPAR $\gamma$ 1 in control (Int-sgRNA) and heterozygous Ex1-sgRNA samples, while no PPAR $\gamma$  bands were detected in the homozygous Ex1-sgRNA or Ex3-sgRNA cells (Figure 1E). The C-terminal PPAR $\gamma$  blot corroborated the PPAR $\gamma$ 1 detection and identified a ~40 kDa band in Ex1-sgRNA cells, matching the predicted size of PPAR $\gamma$  M135, with higher intensity in Ex1-sgRNA -/- cells (Figure 1F). Additional smaller bands may reflect alternative translation initiation sites upstream of p.M135. No PPAR $\gamma$  protein was detected in Ex3-sgRNA -/- cells, indicating complete loss of PPAR $\gamma$  (Figure 1F).

To compare the transcriptional profiles of cells expressing WT and PPAR $\gamma$  M135, the Int-sgRNA +/+ and Ex1-sgRNA -/- clonal cell lines were differentiated into macrophages, stimulated with 1  $\mu$ M rosiglitazone and assessed for gene expression at several canonical PPAR $\gamma$  target genes

(Figure 1G). Upon agonist induction, the Ex1-sgRNA  $-/-$  cells expressed significantly higher levels of *ANGPTL4*(20) ( $p=0.001$ ), *PDK4*(21) ( $p=6.2e-6$ ), and *PLIN2*(22) ( $p=5e-4$ ) than the Int-sgRNA  $+/+$  cells. These PPAR $\gamma$  M135 expressing cells also showed non-significant increases in *CD36* and *FABP4* expression. As PPAR $\gamma$  plays a role in monocyte-to-macrophage differentiation, we measured *CD11b*(23) and *CD68*(24) to assess PMA-induced differentiation as a potential confounder. After PMA treatment, *CD11b* and *CD68* expression increased similarly in Ex1-sgRNA  $-/-$  and Int-sgRNA  $+/+$  cells (Figure S1B).

We subsequently isolated and compared the transactivation potentials of WT and PPAR $\gamma$  M135. A PPRE-driven luciferase reporter(25) and WT PPAR $\gamma$  or PPAR $\gamma$  M135 mRNA were transfected into HEK293s, which have minimal endogenous PPAR $\gamma$  activity(26). In this system, PPAR $\gamma$  M135 activated transcriptional activity more potently than WT when induced with rosiglitazone (Figure S1C). We further compared the stability of PPAR $\gamma$  M135 to WT by performing a cycloheximide chase (27) in the heterozygous Ex1-sgRNA cells that generate both isoforms (Figure S1D). The M135 isoform degraded more slowly than PPAR $\gamma$ 1 (Figure S1E) which could contribute to its enhanced transactivation potential.

### **Ligand-activated PPAR $\gamma$ M135 transactivates target genes more potently than WT PPAR $\gamma$ in THP-1s**

We next sought to isolate the activity of PPAR $\gamma$  M135 and evaluate its effect on global transcriptional profiles in comparison with full-length wild-type (WT) PPAR $\gamma$ . To compare the direct transcriptional responses of M135 and WT, we performed RNA-seq on PPAR $\gamma$  null ( $P\gamma^{-/-}$ ) THP-1 monocytes electroporated with in vitro transcribed mRNA of each of the two PPAR $\gamma$  isoforms; eGFP mRNA was also electroporated as a process control. In preliminary experiments, mRNA amounts for each isoform were titrated to express similar amounts of protein at the point

of harvest (Figure S2A, B), such that 2  $\mu\text{g}$  PPAR $\gamma$  M135 mRNA and 8  $\mu\text{g}$  PPAR $\gamma$  WT were used for each electroporation. The electroporated cells were differentiated into macrophages to mimic the cellular context in which PPAR $\gamma$  is active (28) and treated with 0 (-) and 1  $\mu\text{M}$  (+) rosiglitazone. As a positive control, wild-type (P $\gamma^{+/+}$ ) THP-1 cells with intact *PPARG* were also treated with +/- rosiglitazone and transcriptionally profiled (Figure 2A).

After filtering for low expression, 16,732 transcripts were retained for analysis across all samples. As expected, rosiglitazone treatment increased gene expression of canonical PPAR $\gamma$  target genes including *CD36*, *FABP4* (3), and *PLIN2* (22) (Figure 2B). Remarkably, PPAR $\gamma$  M135-electroporated (P $\gamma^{-/-}$  +M135) cells exhibited greater agonist-induced transcriptional responses for some of these targets compared to P $\gamma^{-/-}$  +WT or P $\gamma^{+/+}$  THP-1 macrophages, despite comparable PPAR $\gamma$  protein levels (log<sub>2</sub> fold-change (log<sub>2</sub>FC): *CD36*: P $\gamma^{-/-}$  +M135=4.22, P $\gamma^{+/+}$  =2.94, P $\gamma^{-/-}$  +WT=1.62. *PLIN2*: P $\gamma^{-/-}$  +M135=3.35, P $\gamma^{+/+}$ =3.24, P $\gamma^{-/-}$  +WT=1.50).

To comprehensively evaluate if M135 generated a stronger agonist-induced transcriptional response than WT in P $\gamma^{-/-}$  cells, we performed a series of differential expression analyses. We first identified the top-ranked PPAR $\gamma$  target genes as defined by the 50 most significant differentially expressed genes (DEGs) in P $\gamma^{+/+}$  cells +/- rosiglitazone and then compared the log<sub>2</sub>FC for the same genes across P $\gamma^{-/-}$  +WT and P $\gamma^{-/-}$  +M135 +/- rosiglitazone (Figure 2C). Of the top 50 P $\gamma^{+/+}$  DEGs, 46 were also differentially expressed in P $\gamma^{-/-}$  +M135 ( $p < 0.05$ , same sign log<sub>2</sub>FC), whereas only 33 were differentially expressed in P $\gamma^{-/-}$  +WT. Moreover, at several key genes, including *PDK4*, *DYSF*, *ANGPTL4*, *ALOX5AP*, and *CYBB* (29–31), P $\gamma^{-/-}$  +M135 had a greater activation or repression than P $\gamma^{+/+}$  cells (Figure 2C) despite transient and lower PPAR $\gamma$  protein expression per cell (Figure S2A, B). Across all the P $\gamma^{+/+}$  DEGs ( $n=1779$ ), the magnitude of gene expression change was more similar for P $\gamma^{-/-}$  +M135 cells (slope=0.85) than for P $\gamma^{-/-}$  +WT cells (slope=0.36),

indicating greater potency of M135 in mediating agonist-induced PPAR $\gamma$  gene expression response than WT (Figure 2D).

We then queried for DEGs specific to PPAR $\gamma$  M135 to assess if the lack of AF-1 domain in M135 resulted in transactivation/repression of genes not regulated by WT PPAR $\gamma$ . In response to rosiglitazone treatment, P $\gamma$ <sup>-/-</sup> +M135 had the greatest number of DEGs (n=4,247, Figure 2E) as compared to P $\gamma$ <sup>-/-</sup> +WT (n=1,794) or P $\gamma$ <sup>+/+</sup> (n=1,779). Of the 4,247 DEGs, 2,313 were exclusive to P $\gamma$ <sup>-/-</sup> +M135 (Figure 2E). To understand the gene expression programs captured by these putative M135-specific genes, we performed gene set overrepresentation analysis (32,33) among the Gene Ontology Biological Process (GO BP) pathways (34,35) and found 28 overrepresented pathways that were confirmed to be altered by rosiglitazone treatment in M135 complemented cells ( $p < 0.05$ ; Table S4). Among these, 21/28 were similarly altered, although to a lesser degree, by rosiglitazone treatment in either WT-electroporated cells or P $\gamma$ <sup>+/+</sup> THP-1s (Figure 2F). Taken together, these analyses suggest that PPAR $\gamma$  M135 regulates similar gene expression programs as WT, but more potently when induced by rosiglitazone, perhaps due to de-repression from the loss of the N-terminal AF-1 domain(36).

### **Human preadipocytes generate PPAR $\gamma$ M135 and more potently upregulate target genes than WT.**

As many of the major metabolic effects of *PPARG* on human physiology occur in adipocytes(8), we evaluated if adipocytes could also generate PPAR $\gamma$  M135 and to what functional consequence. We targeted a human preadipocyte cell line (Simpson-Golabi-Behmel Syndrome (SGBS) (37)) with disruptions in Exon 1, Exon 3, and a *PPARG* intron (Ex1-sgRNA2 cut site at hg38 chr3:12379716, Ex3-sgRNA chr3:12392733, and Int-sgRNA chr3:12363492, Figure 3A, Table S3). The edited cells were treated with inducers of adipocyte differentiation and examined

for PPAR $\gamma$  protein expression, target gene expression, and adipocyte differentiation efficiency. After four days of differentiation, we were able to detect both PPAR $\gamma$  WT and M135 in Exon 1 targeted cells, whereas Exon 3 targeted cells expressed no PPAR $\gamma$ , and control cells only expressed WT PPAR $\gamma$  (Figure 3B, C). These results indicated that, like THP-1 macrophages, SGBS adipocytes are capable of alternatively generating PPAR $\gamma$  M135 in response to disruptive mutations targeted to Exon 1.

To evaluate the ability of preadipocytes expressing PPAR $\gamma$  M135 to activate PPAR $\gamma$  target genes, we queried gene expression of several targets during early adipocyte differentiation (Figure 3D). SGBS preadipocytes that express PPAR $\gamma$  M135 increase expression of *CD36* ( $p=0.022$ ) and *PDK4* ( $p=5.2e-5$ ) to a significantly greater extent than PPAR $\gamma$  WT expressing cells, similar to macrophages (Figure 1G) and showed a trend towards increased expression of *FABP4* ( $p=0.22$ ). Furthermore, we examined adiponectin (*ADIPOQ*), an adipokine and PPAR $\gamma$  target specific to adipocytes(38), and found it also to be significantly upregulated by PPAR $\gamma$  M135 expressing adipocytes ( $p=0.017$ ) compared to WT (Figure 3D). Cells targeted at Exon 3, which expressed no PPAR $\gamma$ , failed to upregulate the expression of any of these genes.

Finally, we characterized the ability of PPAR $\gamma$  M135 expressing SGBS cells to mature into adipocytes and accumulate lipids during differentiation (Figure 3E, F). Exon 1 targeted, PPAR $\gamma$  M135 expressing SGBS differentiated and accumulated lipids at the same rate as control PPAR $\gamma$  WT expressing cells ( $p=0.933$ ), whereas Exon 3 targeted cells had significantly reduced lipid accumulation ( $p=2e-16$ ). These analyses show that like macrophages, human preadipocytes can generate the PPAR $\gamma$  M135 isoform, and the truncated isoform is fully functional in driving differentiation into mature, lipid-laden adipocytes.

### **PPAR $\gamma$ M135 enhances adipocyte insulin response compared to WT**

To isolate the effect of PPAR $\gamma$  M135, we transduced P $\gamma$ <sup>-/-</sup> SBGS cells (i.e. Ex3-sgRNA targeted cells) with doxycycline-inducible WT PPAR $\gamma$ 2 cDNA (SGBS P $\gamma$ <sup>-/-</sup> +WT) or PPAR $\gamma$  M135 cDNA (SGBS P $\gamma$ <sup>-/-</sup> +M135) transgenes and evaluated differentiation/ lipid accumulation and insulin response (**Figure 4A**). These cells only express PPAR $\gamma$  (WT or M135) when treated with doxycycline (**Figure 4B**) and differentiate to a similar degree only when PPAR $\gamma$  is induced (p=0.56, **Figure 4C, D**).

To assess insulin response control (intronic), SGBS P $\gamma$ <sup>-/-</sup> +WT and SGBS P $\gamma$ <sup>-/-</sup> +M135 were differentiated, stimulated with insulin and immunoblotted for phosphorylated Akt (S473; pAkt) and total Akt. In response to insulin, all cell lines phosphorylate Akt, and the response is augmented in doxycycline treated SGBS P $\gamma$ <sup>-/-</sup> +WT and SGBS P $\gamma$ <sup>-/-</sup> +M135 (ANOVA p=1.33e-13, Tukey HSD p<sub>WT, doxycycline</sub>=3.67e-8, p<sub>M135, doxycycline</sub>=3.43e-11, **Figure 4E, F**). Notably, PPAR $\gamma$  M135 expressing adipocytes show increased insulin stimulated Akt phosphorylation compared to both WT (p=0.025) and control SGBS (p=0.045), indicating an enhanced insulin response.

### **Missense mutations that impair AF-1 function increase PPAR $\gamma$ transactivation and may protect against metabolic syndrome in human carriers**

Next, we sought to evaluate the potential in vivo consequence of nonsense mutations in the *PPARG* sequence prior to chr3:12381414 by identifying human carriers of such mutations and performing genotype:phenotype correlation under the hypothesis that carriers would not exhibit insulin resistance given the enhanced molecular activity of PPAR $\gamma$  M135 from AF-1 domain deletion. Across biobanks and databases comprising over 1.2 million individuals with sequencing at the *PPARG* locus, we only found seven carriers of nonsense mutations prior to chr3:12381414

(Table S5). Among these, two had no evidence of metabolic syndrome or insulin resistance past 50 years of age, one had type 2 diabetes, but no ascertainment of insulin resistance or metabolic syndrome, and four had no available phenotypic information.

As the number of human pre-M135 nonsense mutation carriers was insufficient to make robust inferences, we turned to carriers of *PPARG* missense variants to test the hypothesis that genetic variants abrogating AF-1 domain function would enhance PPAR $\gamma$  activity and thereby increase insulin sensitivity in vivo (Figure 5A). While missense variants are not equal to having the M135 isoform, they can model how disruptions to the AF-1 domain affect PPAR $\gamma$  activity in vivo. We rationalized this hypothesis based on recent data that the AF-1 domain intramolecularly binds to the ligand binding domain (LBD) of PPAR $\gamma$ , and this interaction inhibits ligand-dependent activity (36). We identified all carriers of rare (MAF < 0.001) protein-coding variants in *PPARG* in the UK Biobank (UKB, n=454,787) (39) and analyzed the cellular function and amino acid position of the variants carried in relation to the insulin sensitivity-related phenotypes of the individuals carrying them. To quantify PPAR $\gamma$  activity, we leveraged the PPAR $\gamma$  function score (FS) derived from our previously published deep mutational scan(9), in which every possible missense variant was scored by its transactivation of CD36 (9). We found 1,250 carriers of 260 unique rare, protein-coding *PPARG* variants and partitioned them by pre-/post- M135 and by the BLOSUM62 substitution matrix, which quantifies the tolerance of amino acids to substitution across evolutionary distance (40). Variants were categorized as “conservative” (BLOSUM62 > 0) or “non-conservative” (BLOSUM62 < 0). Non-conservative substitutions in AF-1 (FS<sub>median</sub>=2.21) have higher PPAR $\gamma$  FS than conservative substitutions (FS<sub>median</sub>=1.56), while non-conservative substitutions post-M135 in the DBD and LBD (FS<sub>median</sub>=-0.158) show decreased PPAR $\gamma$  FS relative to conservative mutations (FS<sub>median</sub>=-0.376; ANOVA p<2e-16, adjusted p<0.005 for each

pairwise comparison by Tukey HSD; Figure 5B). These data support the hypothesis that missense variants disrupting AF-1 domain function increase the transcriptional activity of PPAR $\gamma$ .

To quantify insulin sensitivity in these *PPARG* missense variant carriers, we computed a per-individual metabolic syndrome severity score (METSS), a measure of insulin sensitivity determined from waist circumference, systolic blood pressure, serum triglycerides, HDL cholesterol, and serum glucose (HbA1c), using methods analogous to those previously published (41–43). We calculated METSS for the 368,911 individuals in the UKB who had all five measurements ascertained, including 908 of the 1250 carriers of rare, protein-coding *PPARG* variants (Figure S3A, B). Of the rare *PPARG* missense variant carriers in the UKB, 340 pre-M135 and 370 post-M135 carriers had computable METSS values. As with the PPAR $\gamma$  function score analysis above (Figure 5B), we partitioned each group into conservative and non-conservative BLOSUM62 to examine the effect of each variant category on METSS (Figure 5C). Under the model that amino acid substitutions that abrogate AF-1 domain function would increase PPAR $\gamma$  activity and thereby decrease METSS, we hypothesized that non-conservative missense variants in AF-1 (pre-M135) would confer lower METSS as compared to conservative amino acid substitutions that would preserve AF-1 function. Conversely, we expected that non-conservative mutations post-M135 in the DBD or LBD would increase METSS, as is the case for lipodystrophy (44). As a positive control, we identified carriers of post-M135 disruptive (i.e. nonsense and frameshift causing) *PPARG* variants (n=14) in our cohort and found their METSS score to be significantly elevated (METSS<sub>median</sub>=1.5, Figure 5D) compared to other *PPARG* variant carriers (ANOVA p=4.1e-6, Tukey p<8.6e-4) and the general UKB population (Welch's t, p=1.1e-4). We observed an ordinal trend with non-conservative, pre-M135 variant carriers having the lowest METSS (METSS<sub>median</sub>=-0.079) followed by conservative, pre-M135 (METSS<sub>median</sub>=0.0064),

conservative, post-M135 ( $\text{METSS}_{\text{median}}=0.24$ ) and finally non-conservative, post-M135 ( $\text{METSS}_{\text{median}}=0.36$ ). The difference between pre- and post-M135 non-conservative variant carriers is significant (Welch's  $t$ ,  $p=0.016$ ).

We performed a similar analysis alternatively utilizing the serum triglyceride to HDL cholesterol (TG/HDL) ratio as a surrogate measure of insulin sensitivity(45,46). The trends observed with METSS were consistent in the TG/HDL results: carriers of post-M135 disruptive (i.e. nonsense and frameshift causing) *PPARG* variants ( $n=15$ ) had the highest values compared to other *PPARG* variant carriers( $\text{TG/HDL}_{\text{median}}=1.65$ , Figure 5D; ANOVA  $p=7.31e-7$ , Tukey HSD  $p<1.1e-4$ ), and the non-conservative, pre-M135 variant carriers had the lowest TG/HDL ( $n=108$ ,  $\text{TG/HDL}_{\text{median}}= -0.080$ ). The difference between pre- and post-M135 non-conservative variant carriers is significant (Welch's  $t$ ,  $p=0.017$ ).

We separately analyzed the well-known *PPARG* p.P12A variant (rs1801282,  $\text{MAF}=0.1050$ ) that is associated with decreased type 2 diabetes risk(47) and occurs frequently in the general population. Under the above partitioning scheme, *PPARG* p.P12A would be classified as pre-M135, non-conservative ( $\text{FS} = 1.3$ , BLOSUM62 score = -1). Carriers of the p.P12A allele ( $n=80,882$ ) in the UKB had significantly decreased METSS (per allele effect size = -0.039,  $p=2e-16$ , Figure S3C, Table S6). These data are suggestive of a model in which AF-1 disrupting variants (both common and rare) can improve insulin sensitivity in vivo.

## Discussion

Here, we characterize a novel isoform of  $\text{PPAR}\gamma$ , termed  $\text{PPAR}\gamma$  M135, which lacks the AF-1 domain and can be generated from an alternative translational start site. In both macrophages and adipocytes,  $\text{PPAR}\gamma$  M135 is transcriptionally active, ligand inducible, and more potent than

WT PPAR $\gamma$ , likely due to de-repression from the loss of the AF-1 domain. We also assess insulin sensitivity in human carriers of *PPARG* variants, demonstrating that variants impairing the AF-1 domain may protect carriers from insulin resistance. Our data support a model for in vivo de-repression of PPAR $\gamma$  in humans that is metabolically beneficial.

Our findings that PPAR $\gamma$  M135 enhances transactivation and improves metabolic health align with studies on naturally occurring and synthetic PPAR $\gamma$  variations. Previous investigations demonstrated that deleting the PPAR $\gamma$  N-terminus increases transcriptional potency compared to WT in NIH-3T3 cells(48,49), and a MAPK phosphorylation site at PPAR $\gamma$  p.S112 inhibits PPAR $\gamma$  transactivation. PPAR $\gamma$  p.S112A, which lacks the phosphorylation site, is more transcriptionally active (50). Additionally, PPAR $\gamma$ 2 p.P12A (rs1801282), which is associated with a reduced risk of type 2 diabetes (47), weakens the interaction between PPAR $\gamma$  and its corepressor NCoR, resulting in increased expression of PPAR $\gamma$  target genes and improved insulin sensitivity in mice (51). Our data corroborate these mechanisms, as METSS scores decrease per p.P12A allele. Furthermore, SUMOylation at p.K107 inhibits ligand-induced transactivation of PPAR $\gamma$  targets (52), and removing that modification increases insulin sensitivity without increasing adiposity in mice (53). Altogether, these studies illustrate that impairing the AF-1 domain increases PPAR $\gamma$  activity and insulin sensitivity.

Regarding therapeutic development, our study proposes a new method to activate PPAR $\gamma$  distinct from TZDs, which target the LBD. We nominate the AF-1 domain as a therapeutic target that is mechanistically distinct from TZDs and SPPARMs, as removing the AF-1 would de-repress rather than activate PPAR $\gamma$ . Accordingly, our data show that adipocytes engineered to produce PPAR $\gamma$  M135 express higher levels of adiponectin, an insulin sensitizing adipokine (54), and have increased Akt phosphorylation in response to insulin stimulation. Further supporting this proposal

are the murine models of human and synthetic *PPARG* variants that increase PPAR $\gamma$  activity via impairing AF-1 (p.P12A(51), p.S112A(55), p.K107(53)), which show enhanced insulin sensitivity compared to WT littermates.

Limitations of our study include the use of in vitro cell models, number of human carriers with analyzable *PPARG* protein-coding variants and generalizability of the UK Biobank population. The THP-1 monocyte and SGBS preadipocyte cell lines, while human, do not fully replicate in vivo conditions, though they have shown consistent results in prior *PPARG* variant studies (8,9,18). Furthermore, PPAR $\gamma$  is active in other tissues including muscle and liver that may have additional metabolic consequences (56,57). These could be the subject of future investigation to fully dissect the metabolic consequences of PPAR $\gamma$  M135. In addition, the number of human carriers of AF-1 domain non-conservative missense variants (n = 94) limits our statistical power to detect changes in metabolic syndrome severity in this group. Moreover, the UK Biobank represents a relatively healthy, middle-aged population of largely British ancestry which is not representative of global populations (58). In the future, our approach can be easily re-applied to larger cohorts and multi-ethnic samples to corroborate and strengthen our findings as they become available to investigators. Another future direction would be to validate the therapeutic hypothesis of generating PPAR $\gamma$  M135 in vivo using transgenic murine models and evaluate tissue specificity.

In summary, we present PPAR $\gamma$  M135, a novel isoform of *PPARG* arising from an alternative translational start site, as a more potent transactivator than full-length PPAR $\gamma$ . This work points to a new mechanism to activate PPAR $\gamma$  by inhibition of the AF-1 domain that could potentially lead to more effective treatments for insulin resistance-related disorders.

## Acknowledgements

We would like to thank the All of Us participants, as the All of Us Research Program would not be possible without their partnership. We are grateful to Angela Liu for technical assistance. Microscopy was performed at the Nikon Imaging Center at UCSD with the support of P. Guo and R. Sanchez. This research has been conducted using the UK Biobank Resource under Application Numbers 41189 and 51436. We would like to acknowledge the participants and the contributions made by the UK Biobank ([www.ukbiobank.ac.uk](http://www.ukbiobank.ac.uk)) in providing the data and resources used in this study.

**Author Contributions.** A.R.M conceived the study. X.D., K.M.-L., and A.R.M. designed the experiments. X.D., K.M.-L., S.H., R.D., G.B., R.H., K.G., C.D.A.S., J.F., S.Heinz and A.R.M. generated/acquired and analyzed the data. X.D., K.M.-L., S.H., R.D., G.B., R.H., J.F., S.Heinz, and A.R.M. were involved in data interpretation. X.D., K.M.-L. and A.R.M. drafted the initial manuscript. All authors were involved in manuscript revision. A.R.M is the guarantor of this work and, as such, had full access to all the data in the study and takes responsibility for the integrity of the data and the accuracy of the data analysis.

**Duality of Interest.** The authors declare no competing interests.

**Funding.** This work was supported by grants from the National Institute of Diabetes and Digestive and Kidney Diseases (1R01DK123422 and R01HL159760 to A.R.M, 1R01DK125490 to J.F and A.R.M) and a UCSD/UCLA Pilot and Feasibility grant (P30 DK063491 to A.R.M). This publication includes data generated at the UC San Diego IGM Genomics Center utilizing an Illumina NovaSeq 6000 that was purchased with funding from a National Institutes of Health SIG grant (#S10 OD026929). The All of Us Research Program is supported by the National Institutes of Health, Office of the Director: Regional Medical Centers: 1 OT2 OD026549; 1 OT2 OD026554;

1 OT2 OD026557; 1 OT2 OD026556; 1 OT2 OD026550; 1 OT2 OD 026552; 1 OT2 OD026553;  
1 OT2 OD026548; 1 OT2 OD026551; 1 OT2 OD026555; IAA #: AOD 16037; Federally Qualified  
Health Centers: HHSN 263201600085U; Data and Research Center: 5 U2C OD023196; Biobank:  
1 U24 OD023121; The Participant Center: U24 OD023176; Participant Technology Systems  
Center: 1 U24 OD023163; Communications and Engagement: 3 OT2 OD023205; 3 OT2  
OD023206; and Community Partners: 1 OT2 OD025277; 3 OT2 OD025315; 1 OT2 OD025337;  
1 OT2 OD025276.

## References

1. James DE, Stöckli J, Birnbaum MJ. The aetiology and molecular landscape of insulin resistance. *Nat Rev Mol Cell Biol.* 2021 Nov;22(11):751–71.
2. Yki-Järvinen H. Thiazolidinediones. *N Engl J Med.* 2004 Aug 27;351(11):1–13.
3. Tontonoz P, Hu E, Graves RA, Budavari AI, Spiegelman BM. mPPAR gamma 2: tissue-specific regulator of an adipocyte enhancer. *Genes Dev.* 1994 May 15;8(10):1224–34.
4. Inzucchi SE, Viscoli CM, Young LH, Furie KL, Gorman M, Lovejoy AM, et al. Pioglitazone Prevents Diabetes in Patients With Insulin Resistance and Cerebrovascular Disease. *Diabetes Care.* 2016 Oct;39(10):1684–92.
5. DePaoli AM, Higgins LS, Henry RR, Mantzoros C, Dunn FL, INT131-007 Study Group. Can a selective PPAR $\gamma$  modulator improve glycemic control in patients with type 2 diabetes with fewer side effects compared with pioglitazone? *Diabetes Care.* 2014 Jul;37(7):1918–23.
6. Savage DB, Tan GD, Acerini CL, Jebb SA, Agostini M, Gurnell M, et al. Human metabolic syndrome resulting from dominant-negative mutations in the nuclear receptor peroxisome proliferator-activated receptor-gamma. *Diabetes.* 2003 Apr;52(4):910–7.
7. Agostini M, Schoenmakers E, Mitchell C, Szatmari I, Savage D, Smith A, et al. Non-DNA binding, dominant-negative, human PPAR $\gamma$  mutations cause lipodystrophic insulin resistance. *Cell Metab.* 2006 Oct 1;4(4):303–11.
8. Majithia AR, Flannick J, Shahinian P, Guo M, Bray MA, Fontanillas P, et al. Rare variants in PPAR $\gamma$  with decreased activity in adipocyte differentiation are associated with increased risk of type 2 diabetes. *Proc Natl Acad Sci U S A.* 2014;111(36):13127–32.
9. Majithia AR, Tsuda B, Agostini M, Gnanapradeepan K, Rice R, Peloso G, et al. Prospective functional classification of all possible missense variants in PPAR $\gamma$ . *Nat Genet.* 2016 Dec;48(12):1570–5.
10. Jiao Y, Ahmed U, Sim MFM, Bejar A, Zhang X, Talukder MMU, et al. Discovering metabolic disease gene interactions by correlated effects on cellular morphology. *Mol Metab.* 2019 Jun;24:108–19.
11. Heinz S, Texari L, Hayes MGB, Urbanowski M, Chang MW, Givarkes N, et al. Transcription Elongation Can Affect Genome 3D Structure. *Cell.* 2018 Sep 6;174(6):1522–36.e22.
12. Robinson MD, McCarthy DJ, Smyth GK. edgeR: a Bioconductor package for differential expression analysis of digital gene expression data. *Bioinformatics.* 2010 Jan 1;26(1):139–40.

13. Law CW, Chen Y, Shi W, Smyth GK. voom: Precision weights unlock linear model analysis tools for RNA-seq read counts. *Genome Biol.* 2014 Feb 3;15(2):R29.
14. Conway JR, Lex A, Gehlenborg N. UpSetR: an R package for the visualization of intersecting sets and their properties. *Bioinformatics.* 2017 Sep 15;33(18):2938–40.
15. Korotkevich G, Sukhov V, Budin N, Shpak B, Artyomov MN, Sergushichev A. Fast gene set enrichment analysis [Internet]. *bioRxiv.* 2021 [cited 2022 Jun 29]. p. 060012. Available from: <https://www.biorxiv.org/content/10.1101/060012v3.full>
16. Cingolani P, Platts A, Wang LL, Coon M, Nguyen T, Wang L, et al. A program for annotating and predicting the effects of single nucleotide polymorphisms, SnpEff: SNPs in the genome of *Drosophila melanogaster* strain w1118; iso-2; iso-3. *Fly.* 2012 Apr-Jun;6(2):80–92.
17. Evangelou E, Warren HR, Mosen-Ansorena D, Mifsud B, Pazoki R, Gao H, et al. Genetic analysis of over 1 million people identifies 535 new loci associated with blood pressure traits. *Nat Genet.* 2018 Oct;50(10):1412–25.
18. Agostini M, Schoenmakers E, Beig J, Fairall L, Szatmari I, Rajanayagam O, et al. A Pharmacogenetic Approach to the Treatment of Patients With PPAR $\gamma$  Mutations. *Diabetes.* 2018 Jun;67(6):1086–92.
19. Tontonoz P, Nagy L, Alvarez JGA, Thomazy VA. PPAR $\gamma$  promotes monocyte/macrophage differentiation and uptake of oxidized LDL. *Cell* [Internet]. 1998; Available from: <https://www.sciencedirect.com/science/article/pii/S0092867400815755>
20. Aryal B, Rotllan N, Araldi E, Ramírez CM, He S, Chousterman BG, et al. ANGPTL4 deficiency in haematopoietic cells promotes monocyte expansion and atherosclerosis progression. *Nat Commun.* 2016 Jul 27;7:12313.
21. Lefterova MI, Zhang Y, Steger DJ, Schupp M, Schug J, Cristancho A, et al. PPAR $\gamma$  and C/EBP factors orchestrate adipocyte biology via adjacent binding on a genome-wide scale. *Genes Dev.* 2008 Nov 1;22(21):2941–52.
22. Hodgkinson CP, Ye S. Microarray analysis of peroxisome proliferator-activated receptor- $\gamma$  induced changes in gene expression in macrophages. *Biochem Biophys Res Commun.* 2003 Aug 29;308(3):505–10.
23. Gažová I, Lefevre L, Bush SJ, Clohisey S, Arner E, de Hoon M, et al. The Transcriptional Network That Controls Growth Arrest and Macrophage Differentiation in the Human Myeloid Leukemia Cell Line THP-1. *Front Cell Dev Biol.* 2020 Jul 3;8:498.
24. Genin M, Clement F, Fattaccioli A, Raes M, Michiels C. M1 and M2 macrophages derived from THP-1 cells differentially modulate the response of cancer cells to etoposide. *BMC Cancer.* 2015 Aug 8;15:577.
25. Kim JB, Wright HM, Wright M, Spiegelman BM. ADD1/SREBP1 activates PPAR $\gamma$

- through the production of endogenous ligand. *Proc Natl Acad Sci U S A*. 1998 Apr 14;95(8):4333–7.
26. Ma JJ, Zhang T, Fang N, Zou Y, Gong QH, Yu LM, et al. Establishment of a cell-based drug screening model for identifying agonists of human peroxisome proliferator-activated receptor gamma (PPAR $\gamma$ ). *J Pharm Pharmacol*. 2012 May;64(5):719–26.
  27. Hsu HY, Nicholson AC, Hajjar DP. Inhibition of macrophage scavenger receptor activity by tumor necrosis factor-alpha is transcriptionally and post-transcriptionally regulated. *J Biol Chem*. 1996 Mar 29;271(13):7767–73.
  28. Rovera G, O'Brien TG, Diamond L. Induction of differentiation in human promyelocytic leukemia cells by tumor promoters. *Science*. 1979 May 25;204(4395):868–70.
  29. de Morrée A, Flix B, Bagaric I, Wang J, van den Boogaard M, Grand Moursel L, et al. Dysferlin regulates cell adhesion in human monocytes. *J Biol Chem*. 2013 May 17;288(20):14147–57.
  30. Pott S, Kamrani NK, Bourque G, Pettersson S, Liu ET. PPARG binding landscapes in macrophages suggest a genome-wide contribution of PU.1 to divergent PPARG binding in human and mouse. *PLoS One*. 2012 Oct 31;7(10):e48102.
  31. Keller MD, Notarangelo LD, Malech HL. Future of Care for Patients With Chronic Granulomatous Disease: Gene Therapy and Targeted Molecular Medicine. *J Pediatric Infect Dis Soc*. 2018 May 9;7(suppl\_1):S40–4.
  32. Chang JT, Nevins JR. GATHER: a systems approach to interpreting genomic signatures. *Bioinformatics*. 2006 Dec 1;22(23):2926–33.
  33. Yu G, Wang LG, Han Y, He QY. clusterProfiler: an R package for comparing biological themes among gene clusters. *OMICS*. 2012 May;16(5):284–7.
  34. Ashburner M, Ball CA, Blake JA, Botstein D, Butler H, Cherry JM, et al. Gene ontology: tool for the unification of biology. The Gene Ontology Consortium. *Nat Genet*. 2000 May;25(1):25–9.
  35. Gene Ontology Consortium. The Gene Ontology resource: enriching a GOLD mine. *Nucleic Acids Res*. 2021 Jan 8;49(D1):D325–34.
  36. Mosure SA, Munoz-Tello P, Kuo KT, MacTavish B, Yu X, Scholl D, et al. Structural basis of interdomain communication in PPAR $\gamma$  [Internet]. *bioRxiv*. 2022 [cited 2023 May 4]. p. 2022.07.13.499031. Available from: <https://www.biorxiv.org/content/10.1101/2022.07.13.499031v1.full>
  37. Wabitsch M, Brenner RE, Melzner I, Braun M, Möller P, Heinze E, et al. Characterization of a human preadipocyte cell strain with high capacity for adipose differentiation. *Int J Obes Relat Metab Disord*. 2001;25(1):8–15.

38. Combs TP, Wagner JA, Berger J, Doebber T, Wang WJ, Zhang BB, et al. Induction of adipocyte complement-related protein of 30 kilodaltons by PPAR $\gamma$  agonists: a potential mechanism of insulin sensitization. *Endocrinology*. 2002 Mar 1;143(3):998–1007.
39. Backman JD, Li AH, Marcketta A, Sun D, Mbatchou J, Kessler MD, et al. Exome sequencing and analysis of 454,787 UK Biobank participants. *Nature*. 2021 Nov;599(7886):628–34.
40. Henikoff S, Henikoff JG. Amino acid substitution matrices from protein blocks. *Proc Natl Acad Sci U S A*. 1992 Nov 15;89(22):10915–9.
41. Gurka MJ, Lilly CL, Oliver MN, DeBoer MD. An examination of sex and racial/ethnic differences in the metabolic syndrome among adults: a confirmatory factor analysis and a resulting continuous severity score. *Metabolism*. 2014 Feb;63(2):218–25.
42. Cavero-Redondo I, Martínez-Vizcaíno V, Álvarez-Bueno C, Agudo-Conde C, Lugones-Sánchez C, García-Ortiz L. Metabolic Syndrome Including Glycated Hemoglobin A1c in Adults: Is It Time to Change? *J Clin Med Res [Internet]*. 2019 Dec 1;8(12). Available from: <http://dx.doi.org/10.3390/jcm8122090>
43. Agarwal S, Jacobs DR Jr, Vaidya D, Sibley CT, Jorgensen NW, Rotter JI, et al. Metabolic Syndrome Derived from Principal Component Analysis and Incident Cardiovascular Events: The Multi Ethnic Study of Atherosclerosis (MESA) and Health, Aging, and Body Composition (Health ABC). *Cardiol Res Pract*. 2012 Mar 21;2012:919425.
44. Jenning EH, Gurnell M, Kalkhoven E. Functional implications of genetic variation in human PPAR $\gamma$ . *Trends Endocrinol Metab*. 2009;20(8):380–7.
45. Oliveri A, Rebernick RJ, Kuppa A, Pant A, Chen Y, Du X, et al. Comprehensive genetic study of the insulin resistance marker TG:HDL-C in the UK Biobank. *Nat Genet*. 2024 Feb;56(2):212–21.
46. DeForest N, Wang Y, Zhu Z, Dron JS, Koesterer R, Natarajan P, et al. Genome-wide discovery and integrative genomic characterization of insulin resistance loci using serum triglycerides to HDL-cholesterol ratio as a proxy. *Nat Commun*. 2024 Sep 14;15(1):8068.
47. Altshuler D, Hirschhorn JN, Klannemark M, Lindgren CM, Vohl MC, Nemesh J, et al. The common PPAR $\gamma$  Pro12Ala polymorphism is associated with decreased risk of type 2 diabetes. *Nat Genet*. 2000 Sep;26(1):76–80.
48. Tontonoz P, Hu E, Spiegelman BM. Stimulation of adipogenesis in fibroblasts by PPAR $\gamma$ 2, a lipid-activated transcription factor. *Cell*. 1994 Dec 30;79(7):1147–56.
49. Hummasti S, Tontonoz P. The peroxisome proliferator-activated receptor N-terminal domain controls isotype-selective gene expression and adipogenesis. *Mol Endocrinol*. 2006 Jun;20(6):1261–75.
50. Adams M, Reginato MJ, Shao D, Lazar MA, Chatterjee VK. Transcriptional activation by

- peroxisome proliferator-activated receptor  $\gamma$  is inhibited by phosphorylation at a consensus mitogen-activated protein kinase site. *J Biol Chem.* 1997;272(8):5128–32.
51. Heikkinen S, Argmann C, Feige JN, Koutnikova H, Champy MF, Dali-Youcef N, et al. The Pro12Ala PPAR $\gamma$ 2 Variant Determines Metabolism at the Gene-Environment Interface. *Cell Metab.* 2009 Jul 1;9(1):88–98.
  52. Pascual G, Fong AL, Ogawa S, Gamliel A, Li AC, Perissi V, et al. A SUMOylation-dependent pathway mediates transrepression of inflammatory response genes by PPAR-gamma. *Nature.* 2005 Sep 29;437(7059):759–63.
  53. Katafuchi T, Holland WL, Kollipara RK, Kittler R, Mangelsdorf DJ, Kliewer SA. PPAR $\gamma$ -K107 SUMOylation regulates insulin sensitivity but not adiposity in mice. *Proc Natl Acad Sci U S A.* 2018 Nov 27;115(48):12102–11.
  54. Stern JH, Rutkowski JM, Scherer PE. Adiponectin, Leptin, and Fatty Acids in the Maintenance of Metabolic Homeostasis through Adipose Tissue Crosstalk. *Cell Metab.* 2016 May 10;23(5):770–84.
  55. Rangwala SM, Rhoades B, Shapiro JS, Rich AS, Kim JK, Shulman GI, et al. Genetic Modulation of PPAR $\gamma$  Phosphorylation Regulates Insulin Sensitivity. *Dev Cell.* 2003 Oct 1;5(4):657–63.
  56. Norris AW, Chen L, Fisher SJ, Szanto I, Ristow M, Jozsi AC, et al. Muscle-specific PPAR $\gamma$ -deficient mice develop increased adiposity and insulin resistance but respond to thiazolidinediones. *J Clin Invest.* 2003 Aug 15;112(4):608–18.
  57. Gavrilova O, Haluzik M, Matsusue K, Cutson JJ, Johnson L, Dietz KR, et al. Liver Peroxisome Proliferator-activated Receptor  $\gamma$  Contributes to Hepatic Steatosis, Triglyceride Clearance, and Regulation of Body Fat Mass \*. *J Biol Chem.* 2003 Sep 5;278(36):34268–76.
  58. Fry A, Littlejohns TJ, Sudlow C, Doherty N, Adamska L, Sprosen T, et al. Comparison of Sociodemographic and Health-Related Characteristics of UK Biobank Participants With Those of the General Population. *Am J Epidemiol.* 2017 Nov 1;186(9):1026–34.

## Figure Legends

### **Figure 1. Functional screens across *PPARG* reveal an alternative translational start site at p.M135.**

**A.** Linear representation of PPAR $\gamma$  indicating start sites for  $\gamma$ 1,  $\gamma$ 2 and novel M135. Guides and cut sites (Ex1-sgRNA; chr3:12379745 and Ex3-sgRNA; chr3:12392733. hg38) of CRISPR/Cas9 monoclonal generated cells are shown. Domain structure of PPAR $\gamma$  protein is represented in colors, and epitopes of the N-terminus and C-terminus antibodies (Abs) are indicated. **B.** A library of 95 guide RNAs (sgRNAs) targeting *PPARG* was generated and transduced into THP-1 monocytes, such that each cell received a single construct. The polyclonal THP-1s were differentiated into macrophages, stimulated with a PPAR $\gamma$  agonist, 1  $\mu$ M rosiglitazone (rosi), and sorted by FACS for expression of PPAR $\gamma$  target CD36 into bins of low (-) and high (+) PPAR $\gamma$  activity (n=5 independent replicate sorts). **C.** Enrichment scores (ES) from the CRISPR screen across *PPARG*. The mean ES for each guide across the 5 sort replicates is plotted along the *PPARG2* cDNA based on its cut site (dot) and predicted termination after a 1 base indel (line). The horizontal purple line is the mean and standard error (se) of the intronic guides (n=18). PPAR $\gamma$  p.M135 is denoted by the vertical line. **D.** Function scores (FS) of insertions/deletions (indels) at each amino acid of PPAR $\gamma$ 2 calculated as previously published (Majithia et al. 2016). FS=0 refers to wild-type activity. **E.** Western blots against the N-terminus and **F.** C-terminus of PPAR $\gamma$  protein were performed to detect PPAR $\gamma$  isoforms from monoclonal cell lines, evidencing that pre-M135 edited cell lines (Ex1) generate truncated PPAR $\gamma$  bands, including the predicted p.M135 at 40 kDa (arrow) as opposed to post-M135 (Ex3) targeted cell lines and intronic cell lines (Int). **G.** Relative expression of PPAR $\gamma$  target genes in *PPARG* targeted monoclonal cell lines, with and without rosiglitazone treatment, with GAPDH as the housekeeping gene and Int-sgRNA edited cells with

0 rosi as control. In response to rosiglitazone, the increases in *ANGPTL4*, *PDK4*, and *PLIN2* for Ex1 edited cells (n=6, cyan) were greater than the increases in the Int edited cells (n=6, purple) (Welch's two-sample t-test on delta Ct values). Non-significant increases in *CD36* and *FABP4* were also observed in Ex1 edited cells.

**Figure 2. PPAR $\gamma$  M135 more potently activates ligand stimulated gene expression as compared to WT.**

**A.** PPAR $\gamma$  WT and M135 mRNA, along with control eGFP mRNA, were generated through *in vitro* transcription and electroporated into PPAR $\gamma$  null (P $\gamma$ <sup>-/-</sup>) THP-1 monocytes. The electroporated cells and wild-type THP-1s (P $\gamma$ <sup>+/+</sup>) were differentiated into macrophages and treated with +/- 1 uM rosiglitazone (rosi) for 30 hours before protein and RNA were collected (n=5/condition). **B.** RNA-seq expression in counts per million (CPM) of *PPARG* and selected PPAR $\gamma$  target genes. In response to rosiglitazone treatment, P $\gamma$ <sup>-/-</sup> +M135 activates *CD36* and *PLIN2* with greater fold change than P $\gamma$ <sup>-/-</sup> +WT and P $\gamma$ <sup>+/+</sup>. \* Benjamini-Hochberg corrected (BH) p<0.01, \*\* BH p<1e-4, \*\*\* BH p<1e-8. **C.** Heatmap of log<sub>2</sub>-fold change (log<sub>2</sub>FC) in response to rosiglitazone for each cell type of the top 50 differentially expressed genes (DEGs) in P $\gamma$ <sup>+/+</sup> THP-1s, as ranked by p-value. Asterisks (\*) indicate DEGs changing in the same direction with BH corrected p < 0.05. **D.** Scatterplot of all 1779 P $\gamma$ <sup>+/+</sup> DEG log<sub>2</sub>FC values, comparing the log<sub>2</sub>FC in P $\gamma$ <sup>+/+</sup> to the log<sub>2</sub>FC in P $\gamma$ <sup>-/-</sup> +WT and P $\gamma$ <sup>-/-</sup> +M135. Regression slopes ( $\beta$ ) are significant (p < 2e-16, \*\*\*) for both, but the P $\gamma$ <sup>-/-</sup> +M135 transcriptional response more closely recapitulates P $\gamma$ <sup>+/+</sup>. **E.** Upset plot of the DEGs per cell type +/- rosiglitazone. Left horizontal bars show total DEGs for each of the three conditions. Filled circles connected by lines indicate intersections among the three conditions and vertical bars show the number of DEGs in the corresponding intersections. **F.** Normalized enrichment scores in the GO BP pathways for P $\gamma$ <sup>-/-</sup> M135 specific genes. Overall

transcriptional pathway activation by  $P\gamma^{+/+}$ ,  $P\gamma^{-/-}$  +WT,  $P\gamma^{-/-}$  +M135 are similar and consistent. Pathway names for the GO IDs are in Table S4.

**Figure 3. Human preadipocytes generate PPAR $\gamma$  M135 and more potently upregulate target genes than WT.** **A.** Simpson-Golabi-Behmel Syndrome (SGBS) cells were transduced with a vector containing Cas9 and a sgRNA targeting PPARG Exon 1 (chr3:12379716), Exon 3 (chr3:12392733), or an intron (chr3:12363492). The preadipocytes were differentiated into adipocytes. **B, C.** Western blot for the N-terminus (B, left) and C-terminus (C, right) of PPAR $\gamma$  in SGBS preadipocytes treated with *PPARG* targeting constructs (A) at 4 days post-differentiation. The Ex1 targeted preadipocytes generate PPAR $\gamma$  M135 at 40 kDa (arrow), while the Ex3 targeted cells do not express any PPAR $\gamma$ . Exon 1 targeted cells also express a band ~50 kDa, consistent with translation initiation at PPAR $\gamma$  p.M53. **D.** Expression of PPAR $\gamma$  target genes at 4 days of differentiation by qPCR. Ex1 targeted cells expressed higher levels of *ADIPOQ*, *CD36*, and *PDK4* compared to control. Ex3 edited cells minimally express all PPAR $\gamma$  target genes. N=6 replicates per sample, p-values from linear models of delta Ct (see Methods for more details). **E, F.** Differentiation time-course for Int, Ex1, and Ex3 targeted SGBS cells at days 0, 4, 8, and 14. Cells were fixed and stored in PBS on their respective collection dates, stained on day 14 for nuclei (DAPI, blue) and lipids (BODIPY, green), and imaged. **E.** Imaged at 40x magnification. Ex1 SGBS differentiate on par with Int, and Ex3 SGBS do not accumulate lipids. Scale bar is 50  $\mu$ m. **F.** Quantification of lipid accumulation in SGBS cells. The data was log-normalized and regressed against genotype and differentiation day to determine the effect of genotype. Ex1 was not different from Int (p=0.933), and Ex3 resulted in a significantly different pace (p = 2e-16).

**Figure 4. PPAR $\gamma$  M135 enhances adipocyte insulin response compared to WT.** **A.** SGBS  $P\gamma^{-/-}$  cells were transduced with doxycycline-inducible vectors expressing PPARG WT and M135.

The preadipocytes were differentiated and treated +/- doxycycline. **B.** PPAR $\gamma$  expression in the SGBS cells. SGBS P $\gamma$ <sup>-/-</sup> cells with PPARG transgenes only express PPAR $\gamma$  when treated with doxycycline. **C, D.** Intronic, SGBS P $\gamma$ <sup>-/-</sup> +WT, and SGBS P $\gamma$ <sup>-/-</sup> +M135 cells were differentiated for 12 days, fixed, stained for nuclei (DAPI, blue) and lipid accumulation (BODIPY, green), and imaged. **C.** Imaged at 40x magnification. PPAR $\gamma$  M135 is sufficient to induce differentiation and lipid uptake in SGBS P $\gamma$ <sup>-/-</sup> cells. Scale bar is 50  $\mu$ m. **D.** Quantification of lipid accumulation. SGBS P $\gamma$ <sup>-/-</sup> +M135 cells accumulate the same amount of lipids as SGBS P $\gamma$ <sup>-/-</sup> +WT (n=12 images/well, 4 wells per genotype, p=0.56, t-test). **E, F.** Intronic, SGBS P $\gamma$ <sup>-/-</sup> +WT, and SGBS P $\gamma$ <sup>-/-</sup> +M135 cells were treated +/- doxycycline, +/- 100 nM insulin for 20 minutes and immunoblotted for phosphorylated Akt (pAkt) and total Akt (n=4 biological replicates). **E.** Representative immunoblot. **F.** The pAkt/Akt intensity ratios were significantly different across the conditions (ANOVA p=1.33e-13). Pairwise comparisons are highlighted between the 100 nM insulin stimulated samples for SGBS P $\gamma$ <sup>-/-</sup> +M135 and SGBS P $\gamma$ <sup>-/-</sup> +WT cells treated with 1  $\mu$ g/mL doxycycline (Tukey HSD p=0.025, \*), SGBS P $\gamma$ <sup>-/-</sup> +M135 + doxycycline and Intronic (p=0.045, \*), and SGBS P $\gamma$ <sup>-/-</sup> +WT + doxycycline and Intronic (p=0.99, ns).

**Figure 5. Human carriers of variants in PPAR $\gamma$  that impair the AF-1 domain are protected from metabolic dysfunction.**

**A.** Cartoon representation of AF-1 hypothesis. Removing or having evolutionarily non-conserved amino acid substitutions in the AF-1 domain prevents/impairs the binding of AF-1 to the ligand binding domain, thereby increasing transcriptional activity. (Cyan: AF-1, Orange: DNA-binding domain (DBD), Pink: Hinge, Blue: Ligand-binding domain (LBD), Green: AF-2). Protein cartoon modeled after the PPAR $\gamma$  crystal structure shown in Mosure et al., 2022. **B.** Function scores (FS) for *PPARG* missense variants (MAF < 0.001) from the UK Biobank (UKB, n = 454,787) by

position (i.e. pre-/post-M135), and evolutionary conservation (conservative: BLOSUM62 < 0, nonconservative: BLOSUM62 > 0) category. Pre-M135 non-conservative variants (n=125 carriers) have the highest function scores ( $FS_{\text{median}}=2.21$ ), followed by pre-M135 conservative (n=338,  $FS_{\text{median}}=1.56$ ), post-M135 conservative (n=345,  $FS_{\text{median}}=-0.158$ ), and post-M135 non-conservative (n=166,  $FS_{\text{median}}=-0.376$ ). All pairwise comparisons between categories are significant by ANOVA ( $p < 2e-16$ , \*\*\*) and Tukey HSD. **C.** Metabolic syndrome severity score (METSS) by position and conservation, as in 5B. Carriers of pre-M135, non-conservative missense variants (n=94,  $METSS_{\text{median}}=-0.079$ ) have lower METSS than carriers of pre-M135 conservative missense variants (n=246,  $METSS_{\text{median}}=0.006$ ), followed by carriers of post-M135 conservative missense variants (n=246,  $METSS_{\text{median}}=0.24$ ), and carriers of post-M135 non-conservative missense variants (n=124,  $METSS_{\text{median}}=0.36$ ). Disruptive variants (i.e. frameshift) post-M135 have the highest METSS of these categories (n=14,  $METSS_{\text{median}}=1.5$ ). There is a significant difference between pre-/post-M135 non-conservative METSS (\*,  $p=0.016$ , Welch's t). # indicates that the disruptive carriers are significantly different from every other category by ANOVA ( $p=4.1e-6$ ) and Tukey HSD ( $p<8.6e-4$ ). These data suggest that missense variants reducing AF-1 function protect carriers from metabolic dysfunction compared to other PPAR $\gamma$  missense variants. **D.** TG/HDL, a measurement for insulin resistance, is plotted by position and conservation. Pre-M135, non-conservative variant carriers have the lowest median TG/HDL (-0.080). The carriers of disruptive variants have significantly higher TG/HDL (#, ANOVA  $p=7.31e-7$ , Tukey HSD  $p<1.1e-4$ ), and there is a significant difference between pre-/post-M135 non-conservative variant carriers (\*,  $p=0.017$ , Welch's t).

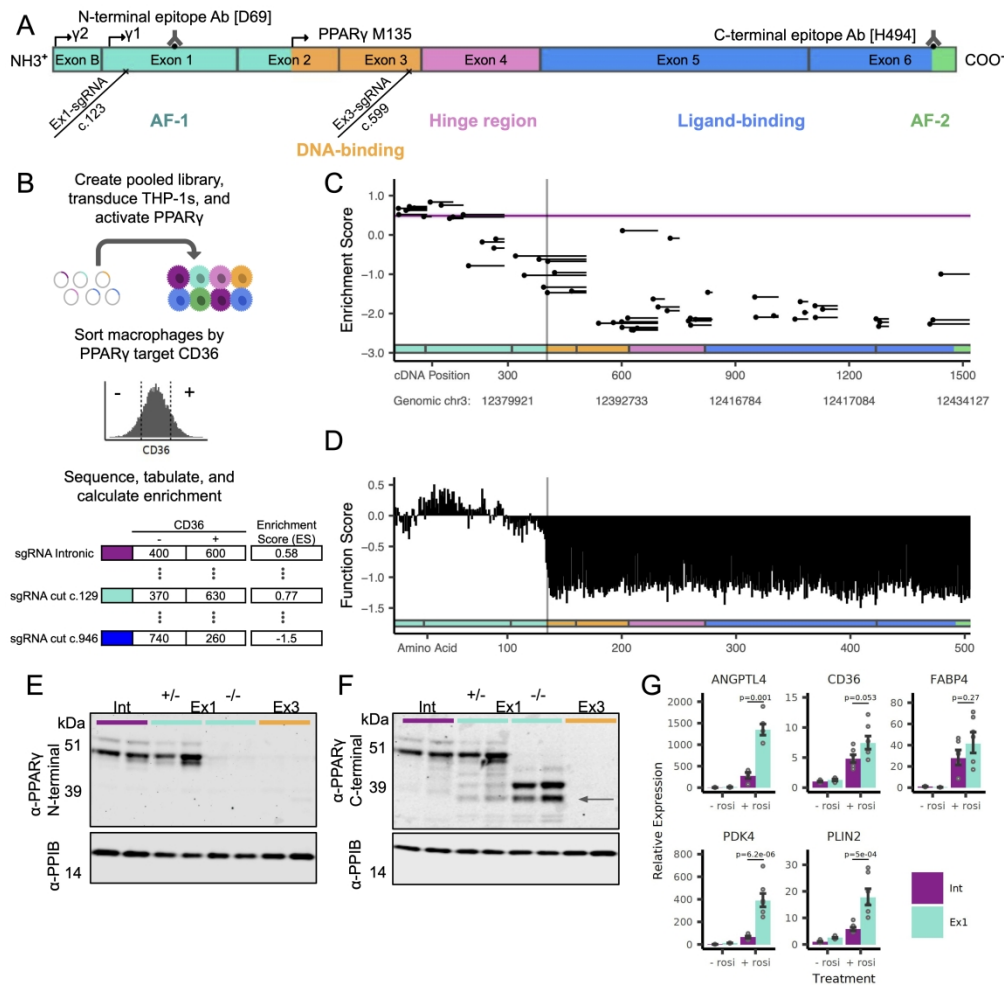


Figure 1. Functional screens across PPAR $\gamma$  reveal an alternative translational start site at p.M135.

A. Linear representation of PPAR $\gamma$  indicating start sites for  $\gamma$ 1,  $\gamma$ 2 and novel M135. Guides and cut sites (Ex1-sgRNA; chr3:12379745 and Ex3-sgRNA; chr3:12392733, hg38) of CRISPR/Cas9 monoclonal generated cells are shown. Domain structure of PPAR $\gamma$  protein is represented in colors, and epitopes of the N-terminus and C-terminus antibodies (Abs) are indicated. B. A library of 95 guide RNAs (sgRNAs) targeting PPAR $\gamma$  was generated and transduced into THP-1 monocytes, such that each cell received a single construct. The polyclonal THP-1s were differentiated into macrophages, stimulated with a PPAR $\gamma$  agonist, 1  $\mu$ M rosiglitazone (rosi), and sorted by FACS for expression of PPAR $\gamma$  target CD36 into bins of low (-) and high (+) PPAR $\gamma$  activity (n=5 independent replicate sorts). C. Enrichment scores (ES) from the CRISPR screen across PPAR $\gamma$ . The mean ES for each guide across the 5 sort replicates is plotted along the PPAR $\gamma$  cDNA based on its cut site (dot) and predicted termination after a 1 base indel (line). The horizontal purple line is the mean and standard error (se) of the intronic guides (n=18). PPAR $\gamma$  p.M135 is denoted by the vertical line. D. Function scores (FS) of insertions/deletions (indels) at each amino acid of PPAR $\gamma$ 2 calculated as previously published (Majithia et al. 2016). FS=0 refers to wild-type activity. E. Western blots against the N-terminus and F. C-terminus of PPAR $\gamma$  protein were performed to detect PPAR $\gamma$  isoforms from monoclonal cell lines, evidencing that pre-M135 edited cell lines (Ex1) generate truncated PPAR $\gamma$  bands, including the predicted p.M135 at 40 kDa (arrow) as opposed to post-M135 (Ex3) targeted cell lines and intronic cell lines (Int). G.

Relative expression of PPAR $\gamma$  target genes in PPAR $\gamma$  targeted monoclonal cell lines, with and without rosiglitazone treatment, with GAPDH as the housekeeping gene and Int-sgRNA edited cells with 0 rosi as control. In response to rosiglitazone, the increases in ANGPTL4, PDK4, and PLIN2 for Ex1 edited cells (n=6, cyan) were greater than the increases in the Int edited cells (n=6, purple) (Welch's two-sample t-test on

delta Ct values). Non-significant increases in CD36 and FABP4 were also observed in Ex1 edited cells.

1491x1492mm (72 x 72 DPI)

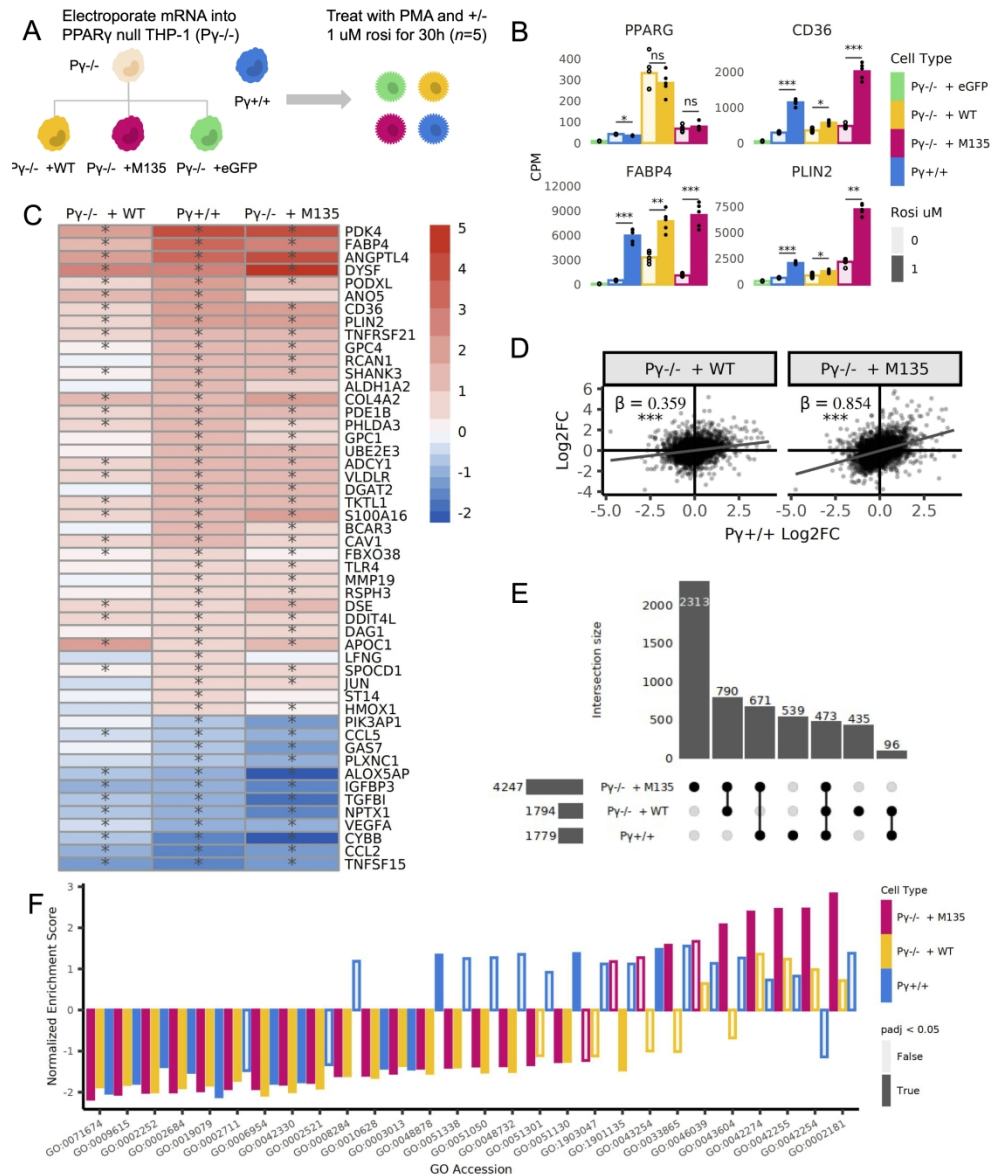


Figure 2. PPAR $\gamma$  M135 more potently activates ligand stimulated gene expression as compared to WT. A. PPAR $\gamma$  WT and M135 mRNA, along with control eGFP mRNA, were generated through in vitro transcription and electroperated into PPAR $\gamma$  null (Py $^{-/-}$ ) THP-1 monocytes. The electroperated cells and wild-type THP-1s (Py $^{+/+}$ ) were differentiated into macrophages and treated with +/- 1  $\mu$ M rosiglitazone (rosi) for 30 hours before protein and RNA were collected (n=5/condition). B. RNA-seq expression in counts per million (CPM) of PPARG and selected PPAR $\gamma$  target genes. In response to rosiglitazone treatment, Py $^{-/-}$  + M135 activates CD36 and PLIN2 with greater fold change than Py $^{-/-}$  + WT and Py $^{+/+}$ . \* Benjamini-Hochberg corrected (BH)  $p < 0.01$ , \*\* BH  $p < 1e-4$ , \*\*\* BH  $p < 1e-8$ . C. Heatmap of log $_2$ -fold change (log $_2$ FC) in response to rosiglitazone for each cell type of the top 50 differentially expressed genes (DEGs) in Py $^{+/+}$  THP-1s, as ranked by p-value. Asterisks (\*) indicate DEGs changing in the same direction with BH corrected  $p < 0.05$ . D. Scatterplot of all 1779 Py $^{+/+}$  DEG log $_2$ FC values, comparing the log $_2$ FC in Py $^{+/+}$  to the log $_2$ FC in Py $^{-/-}$  + WT and Py $^{-/-}$  + M135. Regression slopes ( $\beta$ ) are significant ( $p < 2e-16$ , \*\*\*) for both, but the Py $^{-/-}$  + M135 transcriptional response more closely recapitulates Py $^{+/+}$ . E. Upset plot of the DEGs per cell type +/- rosiglitazone. Left horizontal bars show total DEGs for each of the three conditions. Filled circles connected

by lines indicate intersections among the three conditions and vertical bars show the number of DEGs in the corresponding intersections. F. Normalized enrichment scores in the GO BP pathways for P $\gamma$ <sup>-/-</sup> M135 specific genes. Overall transcriptional pathway activation by P $\gamma$ <sup>+/+</sup>, P $\gamma$ <sup>-/-</sup> +WT, P $\gamma$ <sup>-/-</sup> +M135 are similar and consistent. Pathway names for the GO IDs are in Table S4.

1484x1758mm (72 x 72 DPI)

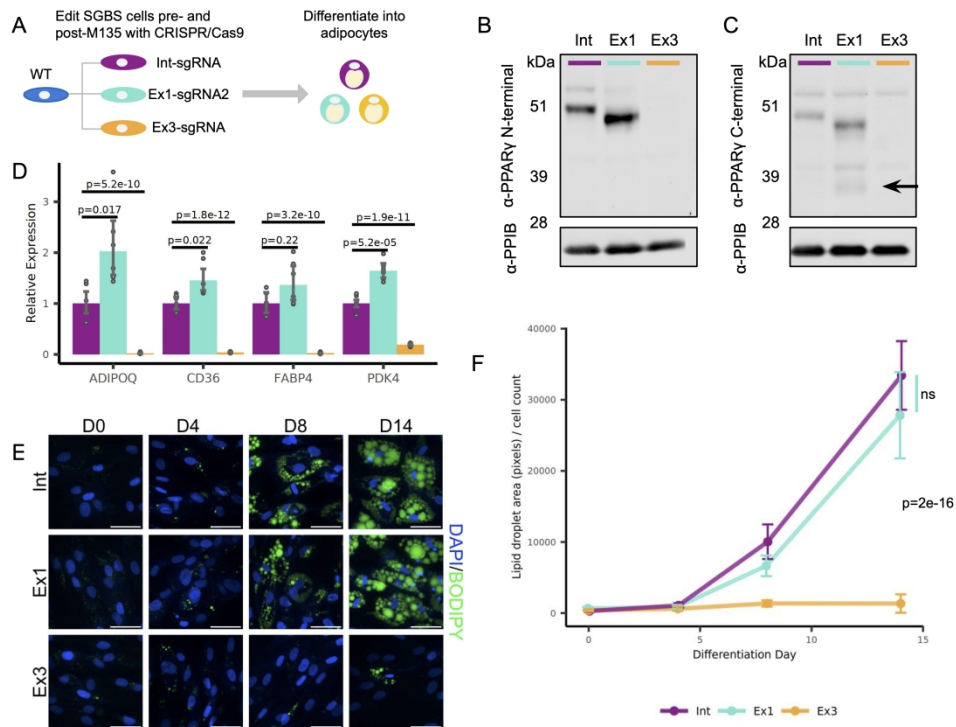


Figure 3. Human preadipocytes generate PPAR $\gamma$  M135 and more potently upregulate target genes than WT. A. Simpson-Golabi-Behmel Syndrome (SGBS) cells were transduced with a vector containing Cas9 and a sgRNA targeting PPAR $\gamma$  Exon 1 (chr3:12379716), Exon 3 (chr3:12392733), or an intron (chr3:12363492). The preadipocytes were differentiated into adipocytes. B, C. Western blot for the N-terminus (B, left) and C-terminus (C, right) of PPAR $\gamma$  in SGBS preadipocytes treated with PPAR $\gamma$  targeting constructs (A) at 4 days post-differentiation. The Ex1 targeted preadipocytes generate PPAR $\gamma$  M135 at 40 kDa (arrow), while the Ex3 targeted cells do not express any PPAR $\gamma$ . Exon 1 targeted cells also express a band ~50 kDa, consistent with translation initiation at PPAR $\gamma$  p.M53. D. Expression of PPAR $\gamma$  target genes at 4 days of differentiation by qPCR. Ex1 targeted cells expressed higher levels of ADIPOQ, CD36, and PDK4 compared to control. Ex3 edited cells minimally express all PPAR $\gamma$  target genes. N=6 replicates per sample, p-values from linear models of delta Ct (see Methods for more details). E, F. Differentiation time-course for Int, Ex1, and Ex3 targeted SGBS cells at days 0, 4, 8, and 14. Cells were fixed and stored in PBS on their respective collection dates, stained on day 14 for nuclei (DAPI, blue) and lipids (BODIPY, green), and imaged. E. Imaged at 40x magnification. Ex1 SGBS differentiate on par with Int, and Ex3 SGBS do not accumulate lipids. Scale bar is 50  $\mu$ m. F. Quantification of lipid accumulation in SGBS cells. The data was log-normalized and regressed against genotype and differentiation day to determine the effect of genotype. Ex1 was not different from Int ( $p=0.933$ ), and Ex3 resulted in a significantly different pace ( $p = 2e-16$ ).

1465x1090mm (72 x 72 DPI)

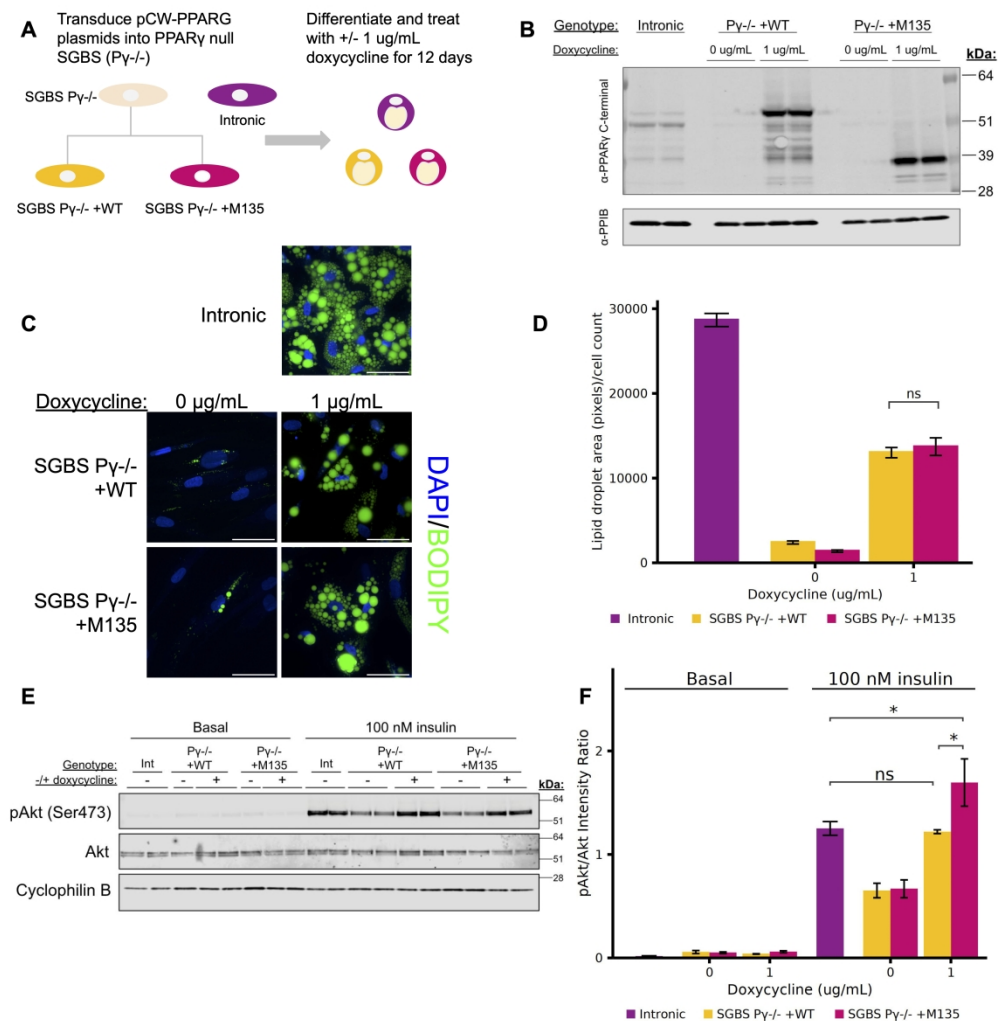


Figure 4. PPAR $\gamma$  M135 enhances adipocyte insulin response compared to WT. A. SGBS P $\gamma$ <sup>-/-</sup> cells were transduced with doxycycline-inducible vectors expressing PPARG WT and M135. The preadipocytes were differentiated and treated +/- doxycycline. B. PPAR $\gamma$  expression in the SGBS cells. SGBS P $\gamma$ <sup>-/-</sup> cells with PPARG transgenes only express PPAR $\gamma$  when treated with doxycycline. C, D. Intrinsic, SGBS P $\gamma$ <sup>-/-</sup> +WT, and SGBS P $\gamma$ <sup>-/-</sup> +M135 cells were differentiated for 12 days, fixed, stained for nuclei (DAPI, blue) and lipid accumulation (BODIPY, green), and imaged. C. Imaged at 40x magnification. PPAR $\gamma$  M135 is sufficient to induce differentiation and lipid uptake in SGBS P $\gamma$ <sup>-/-</sup> cells. Scale bar is 50  $\mu$ m. D. Quantification of lipid accumulation. SGBS P $\gamma$ <sup>-/-</sup> +M135 cells accumulate the same amount of lipids as SGBS P $\gamma$ <sup>-/-</sup> +WT (n=12 images/well, 4 wells per genotype, p=0.56, t-test). E, F. Intrinsic, SGBS P $\gamma$ <sup>-/-</sup> +WT, and SGBS P $\gamma$ <sup>-/-</sup> +M135 cells were treated +/- doxycycline, +/- 100 nM insulin for 20 minutes and immunoblotted for phosphorylated Akt (pAkt) and total Akt (n=4 biological replicates). E. Representative immunoblot. F. The pAkt/Akt intensity ratios were significantly different across the conditions (ANOVA p=1.33e-13). Pairwise comparisons are highlighted between the 100 nM insulin stimulated samples for SGBS P $\gamma$ <sup>-/-</sup> +M135 and SGBS P $\gamma$ <sup>-/-</sup> +WT cells treated with 1  $\mu$ g/mL doxycycline (Tukey HSD p=0.025, \*), SGBS P $\gamma$ <sup>-/-</sup> +M135 + doxycycline and Intrinsic (p=0.045, \*), and SGBS P $\gamma$ <sup>-/-</sup> +WT + doxycycline and Intrinsic (p=0.99, ns).

1471x1530mm (72 x 72 DPI)

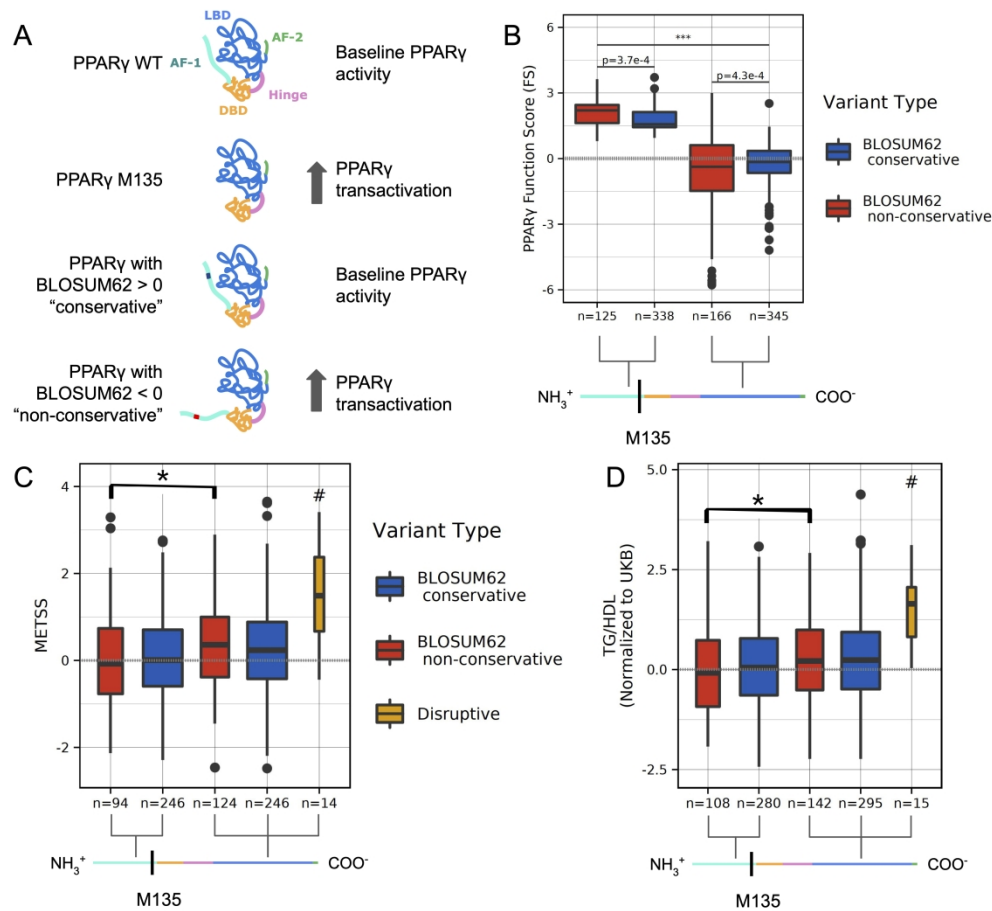
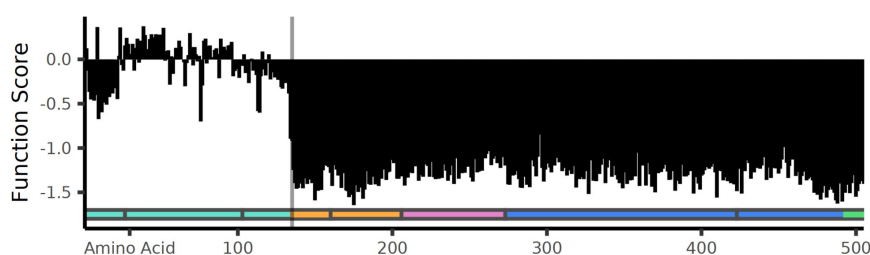


Figure 5. Human carriers of variants in PPAR $\gamma$  that impair the AF-1 domain are protected from metabolic dysfunction. **A**. Cartoon representation of AF-1 hypothesis. Removing or having evolutionarily non-conserved amino acid substitutions in the AF-1 domain prevents/impairs the binding of AF-1 to the ligand binding domain, thereby increasing transcriptional activity. (Cyan: AF-1, Orange: DNA-binding domain (DBD), Pink: Hinge, Blue: Ligand-binding domain (LBD), Green: AF-2). Protein cartoon modeled after the PPAR $\gamma$  crystal structure shown in Mosure et al., 2022. **B**. Function scores (FS) for PPAR $\gamma$  missense variants (MAF < 0.001) from the UK Biobank (UKB, n = 454,787) by position (i.e. pre-/post-M135), and evolutionary conservation (conservative: BLOSUM62 < 0, nonconservative: BLOSUM62 > 0) category. Pre-M135 non-conservative variants (n=125 carriers) have the highest function scores (FSmedian= 2.21), followed by pre-M135 conservative (n=338, FSmedian=1.56), post-M135 conservative (n=345, FSmedian=-0.158), and post-M135 non-conservative (n=166, FSmedian=-0.376). All pairwise comparisons between categories are significant by ANOVA (p < 2e-16, \*\*\*) and Tukey HSD. **C**. Metabolic syndrome severity score (METSS) by position and conservation, as in 5B. Carriers of pre-M135, non-conservative missense variants (n=94, METSSmedian=-0.079) have lower METSS than carriers of pre-M135 conservative missense variants (n=246, METSSmedian=0.006), followed by carriers of post-M135 conservative missense variants (n=246, METSSmedian=0.24), and carriers of post-M135 non-conservative missense variants (n=124, METSSmedian=0.36). Disruptive variants (i.e. frameshift) post-M135 have the highest METSS of these categories (n=14, METSSmedian=1.5). There is a significant difference between pre-/post-M135 non-conservative METSS (\*, p=0.016, Welch's t). # indicates that the disruptive carriers are significantly different from every other category by ANOVA (p=4.1e-6) and Tukey HSD (p<8.6e-4). These data suggest that missense variants reducing AF-1 function protect carriers from metabolic dysfunction compared to other PPAR $\gamma$  missense variants. **D**. TG/HDL, a measurement for insulin resistance, is plotted by position and conservation. Pre-M135, non-conservative variant carriers have the lowest median TG/HDL (-0.080). The

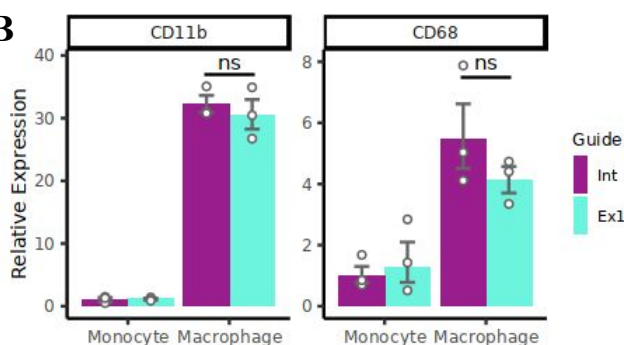
carriers of disruptive variants have significantly higher TG/HDL (#, ANOVA  $p=7.31e-7$ , Tukey HSD  $p<1.1e-4$ ), and there is a significant difference between pre-/post-M135 non-conservative variant carriers (\*,  $p=0.017$ , Welch's t).

1466x1363mm (72 x 72 DPI)

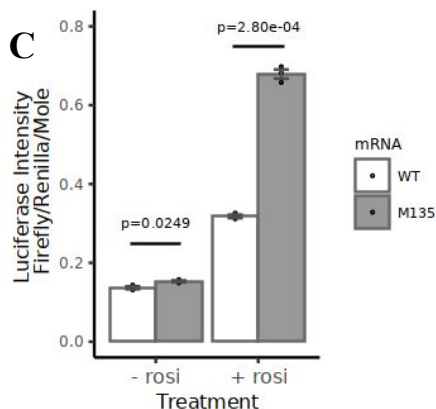
A



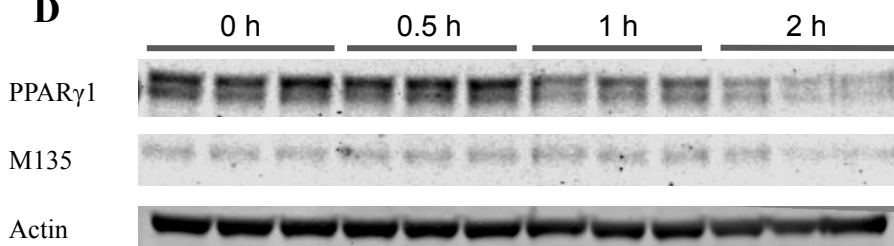
B



C



D



E

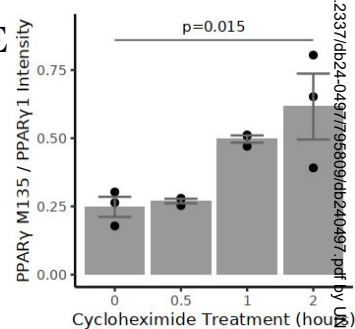


### Figure S1. Related to Figure 1. PPAR $\gamma$ M135 responds to endogenous ligand and degrades more slowly than PPAR $\gamma$ 1.

**A.** Function scores (FS) of insertions/deletions (indels) at each amino acid of PPAR $\gamma$ 2 calculated as previously published (Majithia et al. 2016) after 10  $\mu$ M prostaglandin J2 (PGJ2) treatment. FS=0 refers to wild-type activity. **B.** Relative expression (mean with standard error) of macrophage differentiation markers in intron-edited and Exon 1-edited THP-1 cells, before and after differentiation with 50 ng/mL PMA (n=3 biological replicates per condition). Statistical significance was calculated by a Welch t-test on the delta Ct values for each sample, and the threshold used for significance was p=0.05. **C.** PPRE-driven luciferase promoter activity, normalized to Renilla and by mRNA moles, with 0 and 0.5  $\mu$ M rosiglitazone treatments. PPAR $\gamma$  M135 activates transcription more strongly than WT PPAR $\gamma$  at baseline (n=3 each, t-test) and even more potently when stimulated with rosiglitazone (n=3 each, t-test). **D.** Western blot for the C-terminus of PPAR $\gamma$  in heterozygous Ex1-sgRNA THP-1 cells, which endogenously express both PPAR $\gamma$ 1 and PPAR $\gamma$  M135, after a 0-2 hour treatment with 5  $\mu$ M cycloheximide (n=3). Actin serves as the loading control. **E.** Mean and sem of PPAR $\gamma$  M135/PPAR $\gamma$ 1 measured from D. PPAR $\gamma$  M135/PPAR $\gamma$ 1 increases over time after protein synthesis arrest, indicating slower degradation of PPAR $\gamma$  M135. ANOVA with Tukey post hoc test shows a significant different between 0 and 2 hour time points.

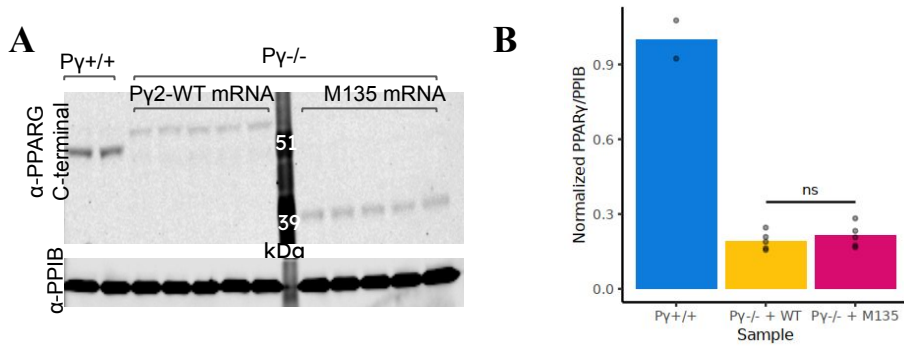


**Figure S2. Related to Figure 2. PPAR $\gamma$  protein abundance in rescue experiments.**

**A.** Western blot for the C-terminus of PPAR $\gamma$  with protein lysates from wild-type THP-1s (P $\gamma$ <sup>+/+</sup>), PPAR $\gamma$  null THP-1s (P $\gamma$ <sup>-/-</sup>) electroporated with PPAR $\gamma$ 2 wild-type (P $\gamma$ 2-WT) mRNA, and P $\gamma$ <sup>-/-</sup> THP-1s electroporated with M135 mRNA. 8 ug WT mRNA and 2 ug M135 mRNA were electroporated to obtain approximately similar protein expression. **B.** Normalized relative abundance of PPAR $\gamma$  protein in P $\gamma$ <sup>+/+</sup> (WT) THP-1, P $\gamma$ <sup>-/-</sup> THP-1 electroporated with WT mRNA, and P $\gamma$ <sup>-/-</sup> THP-1 electroporated with M135 mRNA. The ratio of PPAR $\gamma$  to the loading control of cyclophilin B (PPIB) was normalized to the mean of the P $\gamma$ <sup>+/+</sup> ratios, and data is presented as the mean with the data points. Statistical significance for the difference between P $\gamma$ <sup>-/-</sup> + WT and P $\gamma$ <sup>-/-</sup> + M135 was assessed by a two sample t-test, and the threshold used for significance was p=0.05.

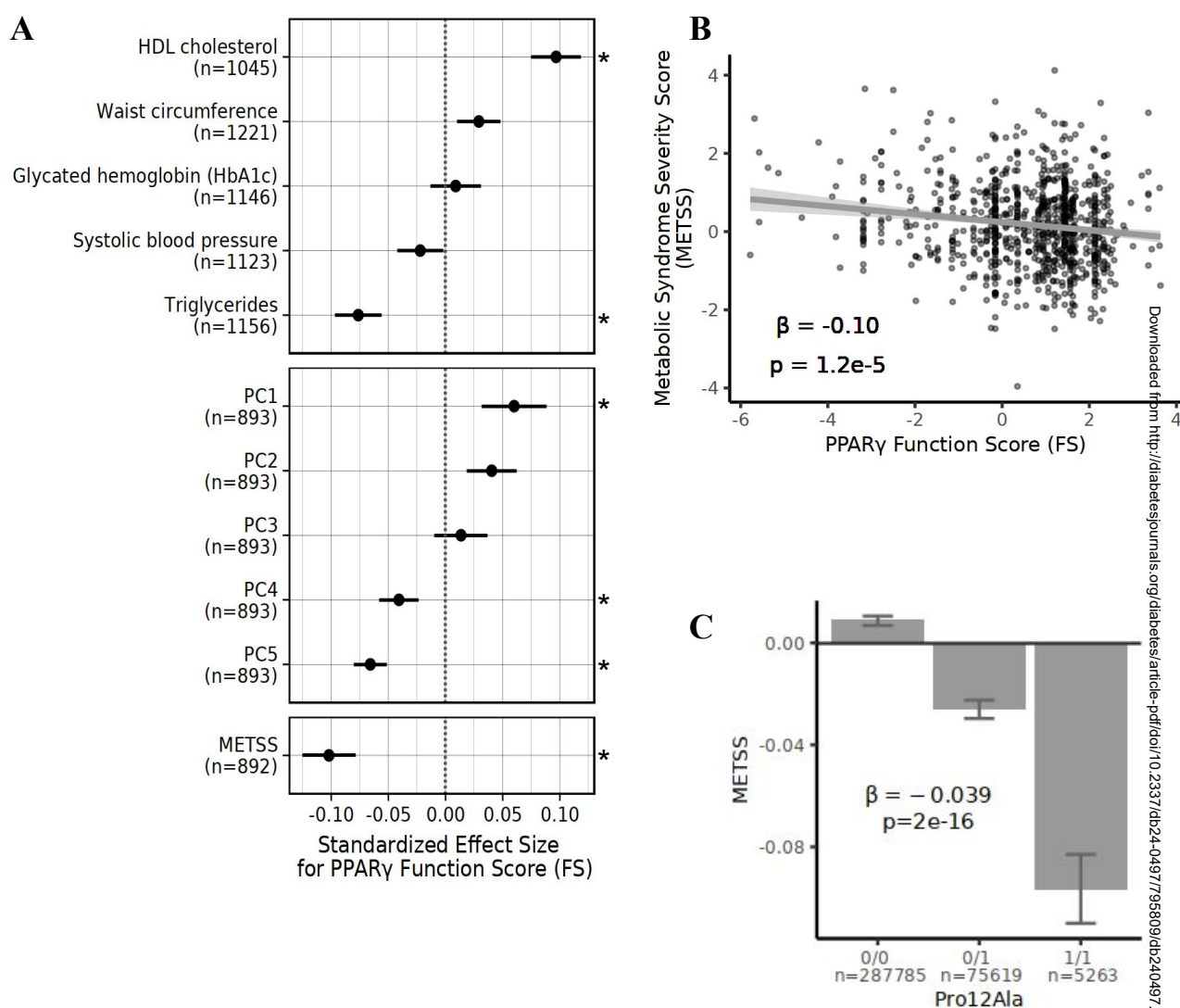


**Figure S3. Related to Figure 5. Aggregation of clinical phenotypes into a metabolic syndrome severity score (METSS).**

**A.** A metabolic syndrome severity score (METSS) was computed from five clinical phenotypes: serum HDL cholesterol, waist circumference, serum triglycerides, systolic blood pressure, and glycated hemoglobin (HbA1c). Regression coefficients for each phenotype against PPAR $\gamma$  function score (FS) are plotted with covariate adjustments for age, age<sup>2</sup>, sex, and 10 genetic principal components. Only serum triglycerides and HDL cholesterol show significant regression slopes. Analogous regression analysis was performed and plotted for principal components (PCs) derived from dimensionality reduction (i.e. PCA) performed on the five clinical phenotypes. PC1, PC4 and PC5 had significant effect sizes when regressed against the PPAR $\gamma$  FS. Standardized effect size (dot) and standard error (lines) are shown for each value; the sample size is the number of individuals with each phenotype/PC and the PPAR $\gamma$  FS, and significance was determined by  $p < 0.05$ . Only 892 individuals were carriers of rare, protein-coding *PPARG* variants with PPAR $\gamma$  FS and had computable METSS. **B.** In carriers of *PPARG* missense variants with METSS (n=892), the metabolic syndrome severity score decreases with increasing PPAR $\gamma$  function (linear regression, effect size = -0.10,  $p=1.2e-5$ ). **C.** Mean and sem of METSS by Pro12Ala genotype. METSS decreases with increasing alleles of the alternate, as modeled by METSS ~ number of alternate alleles, which has effect size of -0.039 and p-value=2e-16.

### THP-1 Cell Culture

Cell suspensions from the human monocytic leukemia cell line THP-1 (ATCC #TIB-202) were cultured in growth media (RPMI 1640 (Gibco, #22400089) + 10% heat-inactivated FBS (Sigma-Aldrich, #F2442) + 1% PenStrep (Gibco, #15140122) + 0.1% 2-Mercaptoethanol (BME; Sigma-Aldrich, #M6250)). In all experiments, cells were differentiated with 50 ng/mL phorbol 12-myristate 13-acetate (PMA; Sigma-Aldrich, #P1585) and PPAR $\gamma$  activation was stimulated with 1  $\mu$ M rosiglitazone (rosi; Cayman Chemicals, #71740). The monoclonal THP-1s were cultured in growth media supplemented with 50% conditioned media (RPMI media harvested from healthy cells at ~70% confluence for 48 hours post the previous passage, clarified by centrifugation at 1000 x g for 10 minutes and then passed through a 0.2  $\mu$ m sterile filter to remove any cell debris).

### Generation of the pooled *PPARG* CRISPR library

To study the effect of insertions and deletions (indels) across *PPARG*, guide RNAs (sgRNAs) (Table S1) were designed using CRISPick (1), ordered as premixed oligos from IDT, phosphorylated, annealed, and ligated into the lentiCRISPRv2 vector (Addgene #52961) through Golden Gate cloning (2). The plasmids were transformed and sequenced for verification. Lentivirus was generated following manufacturer protocols (Mirus Bio #2304) and used to infect THP-1 cells at MOI=0.3 to minimize doubly infected cells, and the edited cells were selected for using 2  $\mu$ g/mL puromycin (Sigma-Aldrich, #P8833). The distribution and efficiency of infection were assessed as follows: genomic DNA (gDNA) was extracted from 1 million cells (Qiagen #51304), split across 4 PCR reactions, amplified (Takara 639208), and loaded onto the iSeq (Illumina), and the reads were deconvolved with PoolQ 3.3.2 (Broad Institute; <https://portals.broadinstitute.org/gpp/public/software/poolq>), which showed a 96.8%

completeness with a maximum of 100x difference between the most over-sequenced guide and the least.

### **Pooled CRISPR experimental assay**

To assess the effect of indels across *PPARG* on its ability to activate a downstream target, the edited THP-1 cells were sorted, alongside wildtype ( $P\gamma^{+/+}$ ) THP-1s and PPAR $\gamma$  null ( $P\gamma^{-/-}$ ) THP-1s, for expression of CD36. To activate PPAR $\gamma$ , the cells were treated with 50 ng/mL PMA for 24h and PMA and 1  $\mu$ M rosi for 48h. The cells were immunostained for CD36 (Miltenyi Biotec, #130-095-472) and sorted using FACS (BD FACSAria II) into two bins: high and low expression of CD36, based on thresholds set by the  $P\gamma^{+/+}$  and  $P\gamma^{-/-}$  cells. 5 independent sorting experiments were performed, sorting ~150,000 cells per bin per replicate. To identify and count the *PPARG* variants in each bin, the methods detailed above were used to extract gDNA, amplify, and sequence. An enrichment score (ES) was generated to quantify the effect of each sgRNA on PPAR $\gamma$  function. The reads for each sorted sample were normalized by library depth, and enrichment was calculated by taking the log<sub>2</sub>-ratio of CD36<sup>+</sup>/CD36<sup>-</sup> normalized counts for each sgRNA.

### **Saturation mutagenesis frameshift analysis**

To determine the impact of indels at each codon of *PPARG*, a function score (FS) for each codon was calculated based on previously published methods(3). The function score is analogous to the CD36<sup>+</sup>/CD36<sup>-</sup> enrichment score described above.

### **Quantitative PCR (qPCR) of monoclonal THP-1 cells**

Ex1-sgRNA <sup>-/-</sup> and Int-sgRNA <sup>+/+</sup> monoclonal cells were seeded in 12-well plates with 750,000 cells per well. 12 wells of each genotype were differentiated with 50 ng/mL PMA for a total of 72 hours, with 6 wells of each genotype additionally receiving 1  $\mu$ M rosi in the last 24 hours.

RNA was extracted (Zymo #R1050) for qPCR. Two independent rounds of seeding and collection were performed. Reverse transcription was performed with the SuperScript III First-Strand Synthesis System (ThermoFisher 18080051) following manufacturer's instructions. Gene expression was analyzed using the iTaq Universal SYBR Green Supermix (Bio-Rad 1725121) with *GAPDH* as the housekeeping gene. Cycle threshold values (Ct) were analyzed using the  $\Delta\Delta C_t$  method(4). Briefly, following outlier removal, technical replicates (n=2) were averaged, and  $\Delta C_t$  values were calculated for each biological replicate along with their mean and standard error (n=3-6 for Figure S1B and Figure 1G). Relative expression (fold-change) was calculated as  $2^{-\Delta\Delta C_t}$  setting a reference condition  $\Delta C_t$  as a calibrator: differentiated Int-sgRNA THP-1s (Figure 1G) and undifferentiated Int-sgRNA THP-1s (Figure S1B). Primer sequences are listed in Table S7.

### **Cycloheximide chase**

3 million THP-1 cells were seeded per well in a 6-well plate and differentiated for 24 hours with 50 ng/mL PMA. Translation was arrested with 5  $\mu$ M cycloheximide, and cells were collected after 0, 0.5, 1, and 2 hours of treatment (n=3). Fifteen  $\mu$ g protein from each sample were loaded into a western blot with the PageRuler Plus Prestained Protein Ladder (Thermo #26619) and immunoblotted with primary antibodies CST #2443 for PPAR $\gamma$  and CST #41185 for actin. Intensities for the PPAR $\gamma$ 1, PPAR $\gamma$  M135, and actin bands were quantified on Image Studio, and the PPAR $\gamma$  intensities for each sample were normalized to its corresponding actin intensity to control for the amount of protein. For each PPAR $\gamma$  isoform, the percentage relative to baseline was calculated by dividing the normalized PPAR $\gamma$  intensity by the mean of that isoform at 0 hours. For each sample, the ratio of PPAR $\gamma$ 1 to PPAR $\gamma$  M135 was obtained by dividing the



Spiegelman). HEK293 cells were seeded 20,000/well and co-transfected with a mixture of 10 ng Renilla (pGL4.75), 10 ng PPREx3-LUC, and 100 ng PPAR $\gamma$  mRNA using Lipofectamine 3000 (Thermo L3000001) for 48 hours. Rosi treated samples were incubated with 0.5  $\mu$ M for 16 hours. Firefly and Renilla luciferase activity was quantified by using the Dual Luciferase Assay System (Promega #E1910), as described by the manufacturer. Luciferase activity was normalized for moles of mRNA transfected.

### **Transcriptomic analysis of THP-1 cell types with exogenous *PPARG* mRNA**

To study the transcriptomes of these cells, RNA was extracted (Zymo #R1050) and sent for library preparation (Illumina Stranded mRNA Prep) and 100 bp paired-end sequencing (25 million reads/sample on the NovaSeq S4). Raw sequencing reads were aligned to the reference hg38 using Kallisto with default parameters (6) to generate gene counts per cell. Analysis was performed in R 4.1.3. EdgeR 3.36.0 and limma-voom (limma v3.50.1) were used to filter and normalize reads for library size and perform differential expression (7,8). UpSetR v1.4.0 was applied to visualize the intersections in differentially expressed genes (DEGs) between the P $\gamma^{+/+}$ , P $\gamma^{+/-}$ M135, and P $\gamma^{+/-}$ WT cell lines in response to rosiglitazone (9,10). To study changes in gene sets, overrepresentation analyses and enrichment analyses were performed in fgsea v1.20.0 (11).

### **Simpson-Golabi-Behmel Syndrome (SGBS) Cell Culture**

SGBS cells were cultured and differentiated into adipocytes following published protocols (12).

### **SGBS qPCR**

QPCR for day 4 differentiation was performed as detailed above for THP-1s. Data were analyzed in aggregate over two separate transductions (batches), each with three biological replicates. To account for multiple biological replicates in two separate batches, relative expression (fold-change) was determined by a linear model of  $\Delta$ Ct  $\sim$  Genotype (Int, Ex1, Ex3) +

Transduction\_Batch, using the intronic targeted samples as reference (i.e. calibrator). The estimate, error, and p-values for Genotype were used as the  $\Delta\Delta C_t$ , standard error, and p-values, respectively, with relative expression calculated as  $2^{-\Delta\Delta C_t}$ . Primer sequences are listed in Table S7.

### **SGBS imaging**

Cells were differentiated for 12 days, fixed in 4% PFA for 10 minutes (Fisher Scientific #50-980-487), permeabilized with 0.1% Triton X-100 (Sigma Aldrich #X100) for 10 minutes, and stained with 5 ug/mL DAPI (Sigma Aldrich #D9542) and 2 ug/mL BODIPY 493/503 (Invitrogen #D3922) for 30 minutes. Images were acquired using a Nikon BioPipeline spinning disk confocal microscope and analyzed using CellProfiler v4.1.3(13).

### **Insulin stimulation**

Day 12 SGBS adipocytes were cultured in insulin-free DMEM F12 for 24 hours prior to stimulation with 100 nM recombinant insulin (Sigma Aldrich #I9278) for 20 minutes in glucose-free Krebs-Ringer buffer as previously described (12). Cells were placed on ice and the insulin-containing buffer was immediately removed prior to washing with cold PBS and cell collection.

### **Human Biobank Data**

UK Biobank (UKB) research was conducted under application numbers 41189 and 51436. Framingham Heart Study (FHS) data was accessed through dbGaP project #30824, “Study on Genetic Risk Scores for Insulin Resistance and their Relation to Metabolic Diseases,” and the All of Us Researcher Workbench was accessed through the workspace, “Detection and analysis of genetic risk factors for insulin resistance v7.” The 1000G variants were accessed through the public data browser(14). The Regeneron Genetics Center Million Exome dataset was accessed through the public variant browser(15), which includes data accessed through UKB application

26041. The Regeneron Genetics Center, and its collaborators (collectively, the “Collaborators”) bear no responsibility for the analyses or interpretations of the data presented here. Any opinions, insights, or conclusions presented herein are those of the authors and not of the Collaborators.

### **Metabolic syndrome severity score (METSS)**

To calculate a continuous score for metabolic syndrome severity, the values of the five constituent clinical phenotypes (16,17), serum HDL cholesterol (field 30760), waist circumference (field 48), serum triglycerides (field 30870), systolic blood pressure (SBP, field 4080), and glycated hemoglobin (HbA1c, field 30750), were extracted for all UKB participants with a complete set of measurements and genetic ancestry data (n=368,911). SBP values were corrected for individuals reported to be taking blood pressure medication by adding 15 mm Hg to the listed measurements (18), and serum triglyceride values were log-normalized. Dimensionality reduction through principal component analysis (R 4.1.3 prcomp) was performed on the corrected values of the phenotypes, and the resulting principal components (PCs) were regressed against PPAR $\gamma$  function score (FS), adjusted for age, age<sup>2</sup>, and sex. The significant PCs were combined into the metabolic syndrome severity score (METSS = PC5 + PC4 - PC1; Figure S3A). The score was adjusted for the covariates of age, age<sup>2</sup>, sex, and the first ten principal components of genetic ancestry, and the residuals were normalized across the UKB participants (n=368,911). The final METSS thus has a mean of 0 and standard deviation of 1 across the UKB, and it has a significant effect size when regressed against the PPAR $\gamma$  FS (Figure S3B). TG/HDL was similarly adjusted and normalized for the UKB participants (n=425,472).

## Supplemental References

1. Doench JG, Fusi N, Sullender M, Hegde M, Vaimberg EW, Donovan KF, et al. Optimized sgRNA design to maximize activity and minimize off-target effects of CRISPR-Cas9. *Nat Biotechnol.* 2016 Feb;34(2):184–91.
2. Engler C, Kandzia R, Marillonnet S. A one pot, one step, precision cloning method with high throughput capability. *PLoS One.* 2008 Nov 5;3(11):e3647.
3. Majithia AR, Tsuda B, Agostini M, Gnanapradeepan K, Rice R, Peloso G, et al. Prospective functional classification of all possible missense variants in PPARG. *Nat Genet.* 2016 Dec;48(12):1570–5.
4. Livak KJ, Schmittgen TD. Analysis of relative gene expression data using real-time quantitative PCR and the 2(-Delta Delta C(T)) Method. *Methods.* 2001 Dec;25(4):402–8.
5. Heinz S, Texari L, Hayes MGB, Urbanowski M, Chang MW, Givarkes N, et al. Transcription Elongation Can Affect Genome 3D Structure. *Cell.* 2018 Sep 6;174(6):1522–36.e22.
6. Bray NL, Pimentel H, Melsted P, Pachter L. Near-optimal probabilistic RNA-seq quantification. *Nat Biotechnol.* 2016 May;34(5):525–7.
7. Robinson MD, McCarthy DJ, Smyth GK. edgeR: a Bioconductor package for differential expression analysis of digital gene expression data. *Bioinformatics.* 2010 Jan 1;26(1):139–40.
8. Law CW, Chen Y, Shi W, Smyth GK. voom: Precision weights unlock linear model analysis tools for RNA-seq read counts. *Genome Biol.* 2014 Feb 3;15(2):R29.
9. Lex A, Gehlenborg N, Strobel H, Vuillemot R, Pfister H. UpSet: Visualization of Intersecting Sets. *IEEE Trans Vis Comput Graph.* 2014 Dec;20(12):1983–92.
10. Conway JR, Lex A, Gehlenborg N. UpSetR: an R package for the visualization of intersecting sets and their properties. *Bioinformatics.* 2017 Sep 15;33(18):2938–40.
11. Korotkevich G, Sukhov V, Budin N, Shpak B, Artyomov MN, Sergushichev A. Fast gene set enrichment analysis [Internet]. *bioRxiv.* 2021 [cited 2022 Jun 29]. p. 060012. Available from: <https://www.biorxiv.org/content/10.1101/060012v3.full>
12. Tews D, Brenner RE, Siebert R, Debatin KM, Fischer-Posovszky P, Wabitsch M. 20 Years with SGBS cells - a versatile in vitro model of human adipocyte biology. *Int J Obes [Internet].* 2022 Aug 19; Available from: <http://dx.doi.org/10.1038/s41366-022-01199-9>
13. Carpenter AE, Jones TR, Lamprecht MR, Clarke C, Kang IH, Friman O, et al. CellProfiler: image analysis software for identifying and quantifying cell phenotypes. *Genome Biol.* 2006 Oct 31;7(10):R100.
14. 1000 Genomes Project Consortium, Auton A, Brooks LD, Durbin RM, Garrison EP, Kang HM, et al. A global reference for human genetic variation. *Nature.* 2015 Oct 1;526(7571):68–74.
15. Sun KY, Bai X, Chen S, Bao S, Kapoor M, Zhang C, et al. A deep catalog of protein-coding variation in 985,830 individuals [Internet]. *bioRxiv.* 2023 [cited 2024 Feb 28]. p. 2023.05.09.539329. Available from: <https://www.biorxiv.org/content/10.1101/2023.05.09.539329v2.full>

16. Gurka MJ, Lilly CL, Oliver MN, DeBoer MD. An examination of sex and racial/ethnic differences in the metabolic syndrome among adults: a confirmatory factor analysis and a resulting continuous severity score. *Metabolism*. 2014 Feb;63(2):218–25.
17. Cavero-Redondo I, Martínez-Vizcaíno V, Álvarez-Bueno C, Agudo-Conde C, Lugones-Sánchez C, García-Ortiz L. Metabolic Syndrome Including Glycated Hemoglobin A1c in Adults: Is It Time to Change? *J Clin Med Res* [Internet]. 2019 Dec 1;8(12). Available from: <http://dx.doi.org/10.3390/jcm8122090>
18. Evangelou E, Warren HR, Mosen-Ansorena D, Mifsud B, Pazoki R, Gao H, et al. Genetic analysis of over 1 million people identifies 535 new loci associated with blood pressure traits. *Nat Genet*. 2018 Oct;50(10):1412–25.

## Captions for Supplementary Tables S1-S7.

<b>Table S1</b>	PPARG CRISPR guides, with columns for guide RNA sequence (sgRNA Sequence), Type, Strand, sgRNA Cut Position on chr3 (1 based; hg38), and mean enrichment scores (ES). Guides are categorized by exonic, intronic, and putative splice variant or UTR variant. The three guides with NA for mean ES were filtered out for low coverage in the libraries.
<b>Table S2</b>	PPARG saturation mutagenesis frameshift data from Majithia et al 2016, with columns for reference amino acid, amino acid position, and PPARγ function score (FS).
<b>Table S3</b>	Guides for CRISPR and primers for genotyping. Cell lines with guides (1) targeted to PPARG intronic sequence (Int-sgRNA), to be used as control, targeted to exon 1 (Ex1-sgRNA), as an example of preM135 edit, and (3) targeted to exon 3 (Ex3-sgRNA), as an example of postM135 edit. Every cell line was screened for genotyping and the gDNA indel was confirmed by sanger sequencing. The location of each guide is indicated in the chromosome coordinates for hg38, and the genotype and protein consequences are relative to PPARγ2 (Uniprot match P37231-1). (n=2 independent clones per group). Ex1-sgRNA 2 was used in the SGBS cells, along with Int-sgRNA and Ex3-sgRNA.
<b>Table S4</b>	Gene set enrichment analysis results across the 3 cell types for the 28 pathways identified by the M135-specific DEGs, with columns for gene ontology set ID (ID), Cell Type, gene ontology pathway name (pathway), p-value (pval), Benjamini-Hochberg corrected p-value (padj), the expected error for standard deviation (log2err), enrichment size (ES), normalized enrichment size (NES), and number of genes from the gene set present in the differential expression analysis.
<b>Table S5</b>	Human variants in PPARG upstream of M135, with columns for variant ID (hg38), Protein Consequence, Database, and Sample Size (n). Each variant encodes a frameshift (fs) that results in a termination (Ter) or a stop codon (*), and the protein consequence is relative to ENSP00000287820.6. The first variant, p.Thr41ProfsTer12, encodes a stop codon at amino acid 52 on Exon 1. The second variant, p.Ile45SerfsTer8, encodes a stop codon at amino acid 52. The third variant, p.Lys63GlnfsTer7, encodes a stop codon at amino acid 69. The fourth variant, p.Ser74TyrfsTer24, results in a stop codon at amino acid 97. The fifth variant, p.Tyr78Ter, encodes a stop codon at amino acid 78. The sixth variant, p.Phe65SerfsTer33, encodes a stop codon at amino acid 97. The seventh variant, p.Gln121*, encodes a stop codon at amino acid 121. All of these occur upstream of p.M135.
<b>Table S6</b>	Metabolic syndrome severity score (METSS) statistics for carriers of PPARG Pro12Ala (rs1801282) in the UKB. Increasing alleles of Ala are associated with decreasing METSS.
<b>Table S7</b>	Primer sequences for qPCR of PPARGγ target genes in THP-1s and SGBS cells. Related to Figure 1G, 3C, and S1B.

**Table S1**

*PPARG* CRISPR guides, with columns for guide RNA sequence (sgRNA Sequence), Type, Strand, sgRNA Cut Position on chr3 (1 based; hg38), and mean enrichment scores (ES). Guides are categorized by exonic, intronic, and putative splice variant or UTR variant. The three guides with NA for mean ES were filtered out for low coverage in the libraries.

sgRNA Sequence	Type	Exon/Intron	Strand	sgRNA Cut Position on chr3 (1 based; hg38)	Mean ES
CCCATAACAGCATGGAATAG	putativeSpliceVariant_ut	B	-	12351581	0.492
ACCCATAACAGCATGGAATA	putativeSpliceVariant_ut	B	-	12351582	0.632
ACCCCTATTCCATGCTGTTA	putativeSpliceVariant_ut	B	+	12351591	0.675
CCCCTATTCCATGCTGTTAT	putativeSpliceVariant_ut	B	+	12351592	0.745
TGCTGTTATGGGTGAAACTC	exonic	B	+	12351603	0.676
GCTGTTATGGGTGAAACTCT	exonic	B	+	12351604	0.518
GAATCGCTTTCTGGGTCAAT	exonic	B	-	12351623	0.625
CAGTGAAGGAATCGCTTTCT	exonic	B	-	12351631	0.664
TCAGTGAAGGAATCGCTTTC	exonic	B	-	12351632	0.722
TGCAGACAGTGTATCAGTGA	exonic	B	-	12351645	0.686
CTGTCTGCAAACATATCACA	exonic	B	+	12351670	0.466
CCCCAATAGCCGTATCTGGA	putativeSpliceVariant_ut	B	-	12351689	0.578
GGATTGCCAACACAAGATCG	intronic	1	+	12356430	0.533
TCTGACTTAAAAGACCCAAG	intronic	1	-	12358443	0.537
AAAGAGCATAGAGTGTCAACA	intronic	1	+	12363492	0.504
AAACTCAGGATACTATGTGA	intronic	1	+	12368774	0.553
CAACCATGGTCATTTCTGAA	putativeSpliceVariant_ut	1	-	12379702	1.213
TGGCATCTCTGTGTCAACCA	exonic	1	-	12379716	0.837
GAGCTGATCCCAAAGTTGGT	exonic	1	-	12379745	0.757
TTCCATTACGGAGAGATCCA	exonic	1	-	12379767	0.419
CTCCGTGGATCTCTCCGTAA	exonic	1	+	12379776	0.459
AGTGAAGGGCTTGATATCAA	exonic	1	-	12379803	0.516
GAGAAGTCAACAGTAGTGAA	exonic	1	-	12379817	-0.785
AATGGAATGTCTTCGTAATG	exonic	1	-	12379853	-0.180
ATTCACAAGAACAGATCCAG	exonic	1	+	12379884	-0.335
TACTTGTAATCTGCAACCAC	exonic	1	-	12379889	-0.103

CAGACTACTAGGACTAGAAT	putativeSpliceVariant_ut	1	+	12379972	0.788
TAATCTTTGACAGAGCGTGG	intronic	2	-	12380770	0.475
ACACCACTGTGAAAAGGTCA	intronic	2	-	12380871	0.484
ACAGTCCTAAAAAGGCAACA	intronic	2	-	12381264	0.386
CTTTTTAGGACTGTTTTTCAT	putativeSpliceVariant_ut	2	+	12381284	NA
TGTGTATGGAGACATGTGAG	putativeSpliceVariant_ut	2	-	12381304	0.195
ATACACAGGTGCAATCAAAG	exonic	2	+	12381331	-0.535
GTCCTTCAGAATAATAAGG	exonic	2	-	12381354	-1.028
GAGTTGGAAGGCTCTTCATG	exonic	2	-	12381393	-0.620
ATTGCCATGAGGGAGTTGGA	exonic	2	-	12381405	-1.329
ACGACATTCAATTGCCATGA	exonic	2	-	12381415	-1.469
CACGACATTCAATTGCCATG	exonic	2	-	12381416	-0.672
GCAATTGAATGTCGTGTCTG	exonic	2	+	12381434	-0.958
TATGGAGTTCATGCTTGTGA	exonic	2	+	12381479	-1.429
TTGGTTAGATTGGCTACACA	intronic	3	+	12383199	0.611
TTCTGGAAGCTACATGATGT	intronic	3	+	12384780	0.419
TGTAAGCCACAACAATGATG	intronic	3	+	12392066	0.302
TTTTAAGTCTTTATGACACA	putativeSpliceVariant_ut	3	-	12392571	0.646
CTTCTTTTTTATCCCTTTC	putativeSpliceVariant_ut	3	+	12392609	0.599
TCCGGAAGAAACCCTGCAA	putativeSpliceVariant_ut	3	-	12392610	-1.193
CTCCGGAAGAAACCCTGCAA	putativeSpliceVariant_ut	3	-	12392611	-1.626
ACAGATGTGATCTTAACTGT	exonic	3	+	12392671	-2.248
GAAATAAATGTCAGTACTGT	exonic	3	+	12392710	-2.231
GTTTCAGAAATGCCTTGCAG	exonic	3	+	12392732	-2.212
TATGAGACATCCCCACTGCA	exonic	3	-	12392733	-2.354
TTCAGAAATGCCTTGCAGTG	exonic	3	+	12392734	0.109
GCAGTGGGGATGTCTCATAA	exonic	3	+	12392748	-2.114
CAATCGGTGGAATTAACCCA	intronic	4	-	12395754	0.345
AAGTTACATACACCGCTGAG	intronic	4	-	12395894	0.547
GTACCTATCTACCTCACGTG	intronic	4	-	12401513	NA
TGGCATCCGCCCAAACCTGA	exonic	4	-	12405888	-2.417

CTATAGCCATCAGGTTTGGG	exonic	4	+	12405893	-2.421
CAGGTTTGGGCGGATGCCAC	exonic	4	+	12405903	-2.373
ATTCAGCTGGTCGATATCAC	exonic	4	-	12405945	-1.631
CAGCGGACTCTGGATTCAGC	exonic	4	-	12405958	-1.834
AATGTTTTGCCAGGGCCCGG	exonic	4	-	12405982	-1.928
GTCATACAAATGTTTTGCCA	exonic	4	-	12405990	-0.084
CTTCCCGCTGACCAAAGCAA	exonic	4	+	12406038	-2.187
CGCTGACCAAAGCAAAGGCG	exonic	4	+	12406043	-2.119
GCTGACCAAAGCAAAGGCGA	exonic	4	+	12406044	-2.297
AAGGCGAGGGCGATCTTGAC	exonic	4	+	12406057	-2.149
CCAGTGTGATCATCGCACCA	intronic	5	-	12410346	0.634
CAGGGGCAGAAACCAACGAG	intronic	5	+	12411793	0.689
AAGCCAATAAAGGCTAGTTG	intronic	5	+	12414337	0.535
GAATGGCTGCAAATAAAACA	putativeSpliceVariant_u	5	-	12416693	-0.689
TTCATGTCATAGATAACGAA	exonic	5	-	12416710	-1.461
GGGCTGCCAGTTTCGCTCCG	exonic	5	+	12416834	-1.580
CTGCCAGTTTCGCTCCGTGG	exonic	5	+	12416837	-2.095
AAGTCAAGATTTACAAAACC	exonic	5	-	12416884	-2.056
GCATTGTGTAATGATCTCG	exonic	5	-	12416940	-2.142
CGAGATCATTTACACAATGC	exonic	5	+	12416954	-1.699
CCCATCTTTATTCATCAAGG	exonic	5	-	12416966	-1.974
AGATGGGGTTCTCATATCCG	exonic	5	+	12416993	-1.804
GATGGGGTTCTCATATCCGA	exonic	5	+	12416994	-2.101
AGGGCCAAGGCTTCATGACA	exonic	5	+	12417013	-1.891
TACATCACTAGGCTTAAGGG	intronic	6	+	12425714	0.312
AAACCATCTTGCCTTAACGG	intronic	6	+	12429087	0.479
GATACCTCACGGTCTAACGG	intronic	6	+	12430380	0.424
GTTTCAGTCAAAAATCCTCT	putativeSpliceVariant_u	6	-	12433848	0.228
CAGCAAACCTGGGCGGTCTG	exonic	6	-	12433898	-2.136
TCACATTCAGCAAACCTGGG	exonic	6	-	12433905	-2.327
GCTTCACATTCAGCAAACCT	exonic	6	-	12433908	-2.220

CAGCTTGGCAAACAGCTGTG	exonic	6	-	12434000	NA
GTTCCGTGACAATCTGTCTG	exonic	6	-	12434040	-2.267
AGACCTCAGACAGATTGTCA	exonic	6	+	12434048	-2.162
GGAACACGTGCAGCTACTGC	exonic	6	+	12434069	-0.996
AACTGGAAGAAGGGAAATGT	putativeSpliceVariant_ut6	6	-	12434172	-0.095
CTTCCAGTTGCACTATTCTG	putativeSpliceVariant_ut6	6	+	12434197	0.315
TTCCAGTTGCACTATTCTGA	putativeSpliceVariant_ut6	6	+	12434198	0.202

**Table S2**

PPARG saturation mutagenesis frameshift data from Majithia et al 2016, with columns for reference amino acid, amino acid position, and PPAR $\gamma$  function score (FS).

Reference PPAR $\gamma$ 2 Amino Acid	PPAR $\gamma$ 2 Amino Acid Position	PPAR $\gamma$ Function Score (FS)
M	1	-0.131
G	2	0.138
E	3	-0.162
T	4	0.129
L	5	0.060
G	6	-0.092
D	7	-0.113
S	8	-0.094
P	9	-0.287
I	10	0.026
D	11	-0.253
P	12	0.062
E	13	-0.253
S	14	-0.383
D	15	-0.180
S	16	-0.037
F	17	0.112
T	18	0.105
D	19	-0.093
T	20	-0.163
L	21	-0.009
S	22	0.020
A	23	0.271
N	24	0.306
I	25	0.071
S	26	0.097
Q	27	0.295

E	28	-0.062
M	29	0.223
T	30	0.159
M	31	0.256
V	32	0.257
D	33	0.118
T	34	0.388
E	35	0.284
M	36	0.509
P	37	0.134
F	38	0.276
W	39	0.199
P	40	0.042
T	41	0.422
N	42	0.332
F	43	0.394
G	44	0.309
I	45	0.445
S	46	0.193
S	47	0.189
V	48	0.431
D	49	0.358
L	50	0.246
S	51	0.268
V	52	0.393
M	53	0.394
E	54	0.197
D	55	0.206
H	56	0.083
S	57	0.061
H	58	0.307

S	59	0.192
F	60	0.208
D	61	0.115
I	62	0.142
K	63	0.071
P	64	0.107
F	65	0.106
T	66	-0.212
T	67	0.179
V	68	0.105
D	69	-0.059
F	70	0.107
S	71	0.090
S	72	0.099
I	73	0.064
S	74	0.114
T	75	0.071
P	76	0.137
H	77	0.033
Y	78	0.440
E	79	0.191
D	80	0.278
I	81	0.099
P	82	0.031
F	83	0.028
T	84	0.101
R	85	-0.127
T	86	0.004
D	87	0.013
P	88	-0.072
V	89	0.125

Downloaded from <http://diabetesjournals.org/diabetes/article-pdf/doi/10.2337/db24-0497> pdf by UNIV OF CALIF SAN DIEGO user on 10 March 2025

V	90	-0.021
A	91	0.149
D	92	0.243
Y	93	0.195
K	94	0.188
Y	95	0.096
D	96	0.120
L	97	-0.174
K	98	-0.107
L	99	0.013
Q	100	-0.053
E	101	-0.228
Y	102	-0.014
Q	103	-0.128
S	104	-0.124
A	105	-0.102
I	106	-0.322
K	107	-0.222
V	108	-0.185
E	109	-0.101
P	110	-0.325
A	111	-0.067
S	112	-0.205
P	113	-0.437
P	114	-0.166
Y	115	-0.161
Y	116	-0.058
S	117	-0.307
E	118	-0.054
K	119	-0.089
T	120	0.038

Q	121	-0.125
L	122	-0.118
Y	123	-0.131
N	124	-0.234
K	125	-0.083
P	126	-0.054
H	127	-0.181
E	128	-0.208
E	129	-0.265
P	130	-0.239
S	131	-0.218
N	132	-0.298
S	133	-0.385
L	134	-0.764
M	135	-0.876
A	136	-1.006
I	137	-1.177
E	138	-1.296
C	139	-1.306
R	140	-1.331
V	141	-1.317
C	142	-1.299
G	143	-1.363
D	144	-1.146
K	145	-1.210
A	146	-1.353
S	147	-1.205
G	148	-1.270
F	149	-0.985
H	150	-1.143
Y	151	-1.206

G	152	-1.423
V	153	-1.218
H	154	-1.147
A	155	-1.219
C	156	-0.517
E	157	-1.145
G	158	-1.102
C	159	-1.227
K	160	-1.181
G	161	-1.194
F	162	-0.954
F	163	-1.032
R	164	-1.183
R	165	-1.087
T	166	-0.585
I	167	-1.337
R	168	-1.164
L	169	-0.884
K	170	-1.194
L	171	-1.263
I	172	-1.319
Y	173	-1.274
D	174	-1.250
R	175	-1.335
C	176	-1.159
D	177	-1.199
L	178	-1.197
N	179	-1.185
C	180	-1.239
R	181	-1.250
I	182	-1.162

H	183	-1.157
K	184	-1.249
K	185	-1.322
S	186	-1.295
R	187	-1.276
N	188	-1.198
K	189	-1.236
C	190	-1.190
Q	191	-1.167
Y	192	-1.182
C	193	-1.154
R	194	-1.234
F	195	-1.150
Q	196	-1.226
K	197	-1.131
C	198	-1.157
L	199	-1.051
A	200	-1.074
V	201	-0.991
G	202	-1.012
M	203	-1.257
S	204	-1.136
H	205	-0.952
N	206	-1.207
A	207	-1.300
I	208	-1.127
R	209	-1.154
F	210	-1.243
G	211	-1.123
R	212	-0.650
M	213	-1.235

P	214	-0.613
Q	215	-1.190
A	216	-1.070
E	217	-1.130
K	218	-1.238
E	219	-1.072
K	220	-1.219
L	221	-1.149
L	222	-1.007
A	223	-1.092
E	224	-1.194
I	225	-0.921
S	226	-1.137
S	227	-1.167
D	228	-1.122
I	229	-1.074
D	230	-1.076
Q	231	-1.125
L	232	-1.224
N	233	-1.116
P	234	-1.076
E	235	-1.213
S	236	-1.216
A	237	-1.124
D	238	-1.158
L	239	-1.106
R	240	-1.402
A	241	-1.073
L	242	-0.969
A	243	-1.120
K	244	-1.065

H	245	-1.139
L	246	-1.279
Y	247	-1.108
D	248	-1.204
S	249	-1.250
Y	250	-1.152
I	251	-1.141
K	252	-1.176
S	253	-1.213
F	254	-0.718
P	255	-0.778
L	256	-1.160
T	257	-0.964
K	258	-1.080
A	259	-1.043
K	260	-1.078
A	261	-0.796
R	262	-1.230
A	263	-1.013
I	264	-1.172
L	265	-0.984
T	266	-1.103
G	267	-1.062
K	268	-1.244
T	269	-0.974
T	270	-1.121
D	271	-1.110
K	272	-1.035
S	273	-1.159
P	274	-1.015
F	275	-1.188

V	276	-1.217
I	277	-1.155
Y	278	-1.177
D	279	-1.130
M	280	-1.215
N	281	-1.312
S	282	-1.334
L	283	-1.135
M	284	-1.207
M	285	-1.059
G	286	-1.036
E	287	-1.184
D	288	-1.242
K	289	-1.157
I	290	-1.447
K	291	-1.253
F	292	-1.088
K	293	-1.164
H	294	-1.055
I	295	-1.081
T	296	-0.651
P	297	-1.145
L	298	-1.210
Q	299	-1.037
E	300	-1.161
Q	301	-0.987
S	302	-1.129
K	303	-1.278
E	304	-1.094
V	305	-1.185
A	306	-0.917

I	307	-1.170
R	308	-1.009
I	309	-1.104
F	310	-0.955
Q	311	-1.172
G	312	-0.975
C	313	-1.064
Q	314	-1.326
F	315	-1.109
R	316	-1.200
S	317	-1.215
V	318	-1.134
E	319	-1.211
A	320	-0.913
V	321	-1.228
Q	322	-1.183
E	323	-1.346
I	324	-1.225
T	325	-1.170
E	326	-1.277
Y	327	-1.317
A	328	-1.095
K	329	-1.236
S	330	-1.243
I	331	-0.899
P	332	-0.810
G	333	-1.162
F	334	-1.193
V	335	-1.071
N	336	-1.217
L	337	-1.030

D	338	-1.094
L	339	-1.290
N	340	-1.221
D	341	-1.035
Q	342	-1.049
V	343	-1.165
T	344	-1.235
L	345	-1.233
L	346	-1.365
K	347	-1.230
Y	348	-1.078
G	349	-1.279
V	350	-1.247
H	351	-1.039
E	352	-1.168
I	353	-1.078
I	354	-1.225
Y	355	-1.160
T	356	-0.814
M	357	-1.116
L	358	-0.993
A	359	-1.017
S	360	-1.353
L	361	-1.054
M	362	-1.336
N	363	-0.943
K	364	-1.109
D	365	-1.159
G	366	-1.222
V	367	-1.217
L	368	-1.115

I	369	-1.184
S	370	-1.201
E	371	-1.159
G	372	-1.074
Q	373	-1.019
G	374	-0.948
F	375	-1.260
M	376	-1.164
T	377	-1.147
R	378	-1.162
E	379	-1.265
F	380	-1.075
L	381	-1.145
K	382	-1.205
S	383	-1.312
L	384	-1.206
R	385	-1.291
K	386	-1.273
P	387	-1.077
F	388	-1.276
G	389	-1.337
D	390	-1.358
F	391	-1.210
M	392	-1.381
E	393	-1.226
P	394	-1.061
K	395	-1.251
F	396	-1.337
E	397	-1.430
F	398	-1.347
A	399	-1.217

V	400	-1.193
K	401	-1.376
F	402	-1.195
N	403	-1.259
A	404	-1.064
L	405	-1.064
E	406	-1.381
L	407	-1.172
D	408	-1.308
D	409	-1.501
S	410	-1.362
D	411	-1.298
L	412	-1.173
A	413	-1.265
I	414	-1.314
F	415	-1.109
I	416	-1.230
A	417	-1.278
V	418	-1.123
I	419	-1.170
I	420	-1.284
L	421	-1.079
S	422	-1.452
G	423	-1.353
D	424	-1.135
R	425	-0.897
P	426	-1.212
G	427	-1.190
L	428	-1.098
L	429	-1.090
N	430	-1.233

V	431	-1.247
K	432	-1.087
P	433	-0.965
I	434	-1.133
E	435	-1.078
D	436	-1.108
I	437	-1.046
Q	438	-1.258
D	439	-1.138
N	440	-1.073
L	441	-1.077
L	442	-1.182
Q	443	-1.160
A	444	-0.870
L	445	-1.077
E	446	-1.173
L	447	-1.155
Q	448	-1.312
L	449	-0.470
K	450	-1.142
L	451	-1.076
N	452	-1.023
H	453	-0.989
P	454	-1.190
E	455	-1.236
S	456	-1.310
S	457	-1.246
Q	458	-1.152
L	459	-1.131
F	460	-1.096
A	461	-1.219

K	462	-1.211
L	463	-1.424
L	464	-1.297
Q	465	-1.190
K	466	-1.290
M	467	-1.178
T	468	-1.266
D	469	-1.232
L	470	-1.151
R	471	-1.252
Q	472	-1.344
I	473	-1.314
V	474	-1.145
T	475	-1.263
E	476	-1.187
H	477	-1.264
V	478	-1.328
Q	479	-1.334
L	480	-1.176
L	481	-1.337
Q	482	-1.372
V	483	-1.134
I	484	-1.168
K	485	-1.300
K	486	-1.311
T	487	-1.156
E	488	-1.256
T	489	-1.148
D	490	-1.308
M	491	-1.276
S	492	-1.149

L	493	-1.281
H	494	-0.805
P	495	-1.321
L	496	-1.289
L	497	-1.418
Q	498	-1.132
E	499	-1.289
I	500	-1.367
Y	501	-1.344
K	502	-1.208
D	503	-1.307
L	504	-1.340
Y	505	-1.197

**Table S3**

Guides for CRISPR and primers for genotyping. Cell lines with guides (1) targeted to PPARG intronic sequence (Int-sgRNA), to be used as control, targeted to exon 1 (Ex1-sgRNA), as an example of preM135 edit, and (3) targeted to exon 3 (Ex3-sgRNA), as an example of postM135 edit. Every cell line was screened for genotyping and the gDNA indel was confirmed by sanger sequencing. The location of each guide is indicated in the chromosome coordinates for hg38, and the genotype and protein consequences are relative to PPARG2 (Uniprot match P37231-1). (n=2 independent clones per group). Ex1-sgRNA 2 was used in the SGBS cells, along with Int-sgRNA and Ex3-sgRNA.

Guide	Chromosomal Location (hg38)	Guide Sequence	Primers	Zygoty
Int-sgRNA	chr3:1236349 2	AAAGAGCATAGAGTGTCACA		+/+
Ex1-sgRNA	chr3:1237974 5	GAGCTGATCCCAAAGTTGGT	FWD: TGAAACTCTGTGAGATTGCTGTGT REV: TGGACTCATCTCTCAGTAACCCT	+/-
				-/-
Ex3-sgRNA	chr3:1239273 3	TATGAGACATCCCCACTGCA	FWD: ACTTTGCCAGGCTGCTTAGCACA REV: TCTCTCTGTGGTTGGGCATCTGC	-/-
Ex1-sgRNA2	chr3:12379716	TGGCATCTCTGTGTCAACCA	FWD: TGAAACTCTGTGAGATTGCTGTGT REV: TGGACTCATCTCTCAGTAACCCT	

Genotype	Protein Consequence
-	-
chr3:12379749_12379751delo12379744_12379750del	p.N42GfsX50
chr3:12379736_12379744delo12379741_12379751del	p.T41SfsX48
chr3:12379744_12379973del	p.PPAR $\gamma$ $\Delta$ 1 (deletion exon 1)
chr3:12379702_12379773del	p.PPAR $\gamma$ $\Delta$ 1 (deletion exon 1)
chr3:12392733insA	p.V201SfsX206
chr3:12392733insT	p.V201GfsX206

Gene set enrichment analysis results across the 3 cell types for the 28 pathways identified by the M135-specific DEGs, with columns for gene ontology set ID (ID), Cell Type, gene ontology pathway name (pathway), Benjamini-Hochberg corrected p-value (padj), normalized enrichment score (NES), and number of genes from the gene set present in the differential expression analysis (size).

**Table S4**

ID	Cell Type	pathway	padj	NES	size
GO:0043604	Pγ+/+	GOBP_AMIDE_BIOSYNTHETIC_PROCESS	9.837E-02	1.264E+00	711
GO:1901135	Pγ+/+	GOBP_CARBOHYDRATE_DERIVATIVE_METABOLIC_PROCESS	3.160E-01	1.121E+00	799
GO:0051301	Pγ+/+	GOBP_CELL_DIVISION	8.181E-01	9.149E-01	540
GO:0048878	Pγ+/+	GOBP_CHEMICAL_HOMEOSTASIS	3.199E-02	1.336E+00	793
GO:0003013	Pγ+/+	GOBP_CIRCULATORY_SYSTEM_PROCESS	2.173E-02	-1.440E+00	383
GO:0002181	Pγ+/+	GOBP_CYTOPLASMIC_TRANSLATION	1.857E-01	1.379E+00	144
GO:0048732	Pγ+/+	GOBP_GLAND_DEVELOPMENT	1.048E-01	1.351E+00	296
GO:0046039	Pγ+/+	GOBP_GTP_METABOLIC_PROCESS	4.907E-01	1.134E+00	21
GO:0002252	Pγ+/+	GOBP_IMMUNE_EFFECTOR_PROCESS	3.016E-02	-1.376E+00	419
GO:0006954	Pγ+/+	GOBP_INFLAMMATORY_RESPONSE	5.080E-06	-1.782E+00	538
GO:0002521	Pγ+/+	GOBP_LEUKOCYTE_DIFFERENTIATION	5.503E-02	-1.329E+00	419
GO:1903047	Pγ+/+	GOBP_MITOTIC_CELL_CYCLE_PROCESS	3.268E-01	1.123E+00	651
GO:0071674	Pγ+/+	GOBP_MONONUCLEAR_CELL_MIGRATION	1.693E-04	-2.019E+00	137
GO:0033865	Pγ+/+	GOBP_NUCLEOSIDE_BISPHOSPHATE_METABOLIC_PROCESS	9.070E-02	1.551E+00	100
GO:0051130	Pγ+/+	GOBP_POSITIVE_REGULATION_OF_CELLULAR_COMPONENT_ORGANIZATION	1.551E-02	1.375E+00	822
GO:0008284	Pγ+/+	GOBP_POSITIVE_REGULATION_OF_CELL_POPULATION_PROLIFERATION	2.257E-01	1.184E+00	642
GO:0010628	Pγ+/+	GOBP_POSITIVE_REGULATION_OF_GENE_EXPRESSION	2.093E-03	-1.413E+00	828
GO:0002684	Pγ+/+	GOBP_POSITIVE_REGULATION_OF_IMMUNE_SYSTEM_PROCESS	7.555E-04	-1.515E+00	616
GO:0051050	Pγ+/+	GOBP_POSITIVE_REGULATION_OF_TRANSPORT	8.926E-02	1.273E+00	645
GO:0002711	Pγ+/+	GOBP_POSITIVE_REGULATION_OF_T_CELL_MEDIATED_IMMUNITY	1.707E-01	-1.474E+00	47
GO:0043254	Pγ+/+	GOBP_REGULATION_OF_PROTEIN_CONTAINING_COMPLEX_ASSEMBLY	2.154E-02	1.473E+00	334

GO:0051338	P $\gamma$ +/+	GOBP_REGULATION_OF_TRANSFERASE_ACTIVITY	1.159E-01	1.254E+00	726
GO:0009615	P $\gamma$ +/+	GOBP_RESPONSE_TO_VIRUS	1.749E-04	-1.785E+00	307
GO:0042274	P $\gamma$ +/+	GOBP_RIBOSOMAL_SMALL_SUBUNIT_BIOGENESIS	9.504E-01	7.280E-01	73
GO:0042255	P $\gamma$ +/+	GOBP_RIBOSOME_ASSEMBLY	8.252E-01	8.273E-01	59
GO:0042254	P $\gamma$ +/+	GOBP_RIBOSOME_BIOGENESIS	2.963E-01	-1.140E+00	298
GO:0042330	P $\gamma$ +/+	GOBP_TAXIS	3.200E-05	-1.749E+00	407
GO:0019079	P $\gamma$ +/+	GOBP_VIRAL_GENOME_REPLICATION	1.917E-04	-2.109E+00	114
GO:0043604	P $\gamma$ -/- +	GOBP_AMIDE_BIOSYNTHETIC_PROCESS	1.330E-17	2.072E+00	711
GO:1901135	P $\gamma$ -/- + M135	GOBP_CARBOHYDRATE_DERIVATIVE_METABOLIC_PROCESS	7.703E-02	1.180E+00	799
GO:0051301	P $\gamma$ -/- +	GOBP_CELL_DIVISION	3.367E-02	-1.328E+00	540
GO:0048878	P $\gamma$ -/- +	GOBP_CHEMICAL_HOMEOSTASIS	1.873E-03	-1.416E+00	793
GO:0003013	P $\gamma$ -/- +	GOBP_CIRCULATORY_SYSTEM_PROCESS	1.487E-03	-1.536E+00	383
GO:0002181	P $\gamma$ -/- +	GOBP_CYTOPLASMIC_TRANSLATION	9.810E-19	2.829E+00	144
GO:0048732	P $\gamma$ -/- +	GOBP_GLAND_DEVELOPMENT	3.293E-02	-1.361E+00	296
GO:0046039	P $\gamma$ -/- +	GOBP_GTP_METABOLIC_PROCESS	6.828E-02	1.666E+00	21
GO:0002252	P $\gamma$ -/- +	GOBP_IMMUNE_EFFECTOR_PROCESS	1.260E-10	-2.004E+00	419
GO:0006954	P $\gamma$ -/- +	GOBP_INFLAMMATORY_RESPONSE	6.480E-10	-1.911E+00	538
GO:0002521	P $\gamma$ -/- +	GOBP_LEUKOCYTE_DIFFERENTIATION	2.990E-06	-1.760E+00	419
GO:1903047	P $\gamma$ -/- +	GOBP_MITOTIC_CELL_CYCLE_PROCESS	8.899E-02	-1.225E+00	651
GO:0071674	P $\gamma$ -/- +	GOBP_MONONUCLEAR_CELL_MIGRATION	9.370E-08	-2.164E+00	137
GO:0033865	P $\gamma$ -/- + M135	GOBP_NUCLEOSIDE_BISPHOSPHATE_METABOLIC_PROCESS	2.345E-02	1.574E+00	100
GO:0051130	P $\gamma$ -/- + M135	GOBP_POSITIVE_REGULATION_OF_CELLULAR_COMPONENT_ORGANIZATION	4.146E-02	-1.255E+00	822
GO:0008284	P $\gamma$ -/- + M135	GOBP_POSITIVE_REGULATION_OF_CELL_POPULATION_PROLIFERATION	3.760E-05	-1.593E+00	642
GO:0010628	P $\gamma$ -/- +	GOBP_POSITIVE_REGULATION_OF_GENE_EXPRESSION	2.530E-06	-1.591E+00	828
GO:0002684	P $\gamma$ -/- + M135	GOBP_POSITIVE_REGULATION_OF_IMMUNE_SYSTEM_PROCESS	1.710E-14	-1.994E+00	616
GO:0051050	P $\gamma$ -/- +	GOBP_POSITIVE_REGULATION_OF_TRANSPORT	9.296E-03	-1.364E+00	645
GO:0002711	P $\gamma$ -/- + M135	GOBP_POSITIVE_REGULATION_OF_T_CELL_MEDIATED_IMMUNITY	2.935E-03	-1.911E+00	47

GO:0043254	Pγ-/- + M135	GOBP_REGULATION_OF_PROTEIN_CONTAINING_COMPLEX_ASSEMBLY	7.703E-02	1.271E+00	334
GO:0051338	Pγ-/- +	GOBP_REGULATION_OF_TRANSFERASE_ACTIVITY	5.777E-03	-1.393E+00	726
GO:0009615	Pγ-/- +	GOBP_RESPONSE_TO_VIRUS	1.170E-09	-2.052E+00	307
GO:0042274	Pγ-/- +	GOBP_RIBOSOMAL_SMALL_SUBUNIT_BIOGENESIS	1.870E-07	2.384E+00	73
GO:0042255	Pγ-/- +	GOBP_RIBOSOME_ASSEMBLY	7.330E-08	2.448E+00	59
GO:0042254	Pγ-/- +	GOBP_RIBOSOME_BIOGENESIS	3.570E-17	2.461E+00	298
GO:0042330	Pγ-/- +	GOBP_TAXIS	8.450E-07	-1.808E+00	407
GO:0019079	Pγ-/- +	GOBP_VIRAL_GENOME_REPLICATION	4.670E-05	-1.964E+00	114
GO:0043604	Pγ-/- + WT	GOBP_AMIDE_BIOSYNTHETIC_PROCESS	1.000E+00	-6.805E-01	711
GO:1901135	Pγ-/- + WT	GOBP_CARBOHYDRATE_DERIVATIVE_METABOLIC_PROCESS	2.106E-04	-1.460E+00	799
GO:0051301	Pγ-/- + WT	GOBP_CELL_DIVISION	3.457E-01	-1.109E+00	540
GO:0048878	Pγ-/- + WT	GOBP_CHEMICAL_HOMEOSTASIS	2.120E-05	-1.541E+00	793
GO:0003013	Pγ-/- + WT	GOBP_CIRCULATORY_SYSTEM_PROCESS	4.384E-02	-1.348E+00	383
GO:0002181	Pγ-/- + WT	GOBP_CYTOPLASMIC_TRANSLATION	9.980E-01	7.167E-01	144
GO:0048732	Pγ-/- + WT	GOBP_GLAND_DEVELOPMENT	7.775E-03	-1.497E+00	296
GO:0046039	Pγ-/- + WT	GOBP_GTP_METABOLIC_PROCESS	9.670E-01	6.425E-01	21
GO:0002252	Pγ-/- + WT	GOBP_IMMUNE_EFFECTOR_PROCESS	1.930E-10	-1.994E+00	419
GO:0006954	Pγ-/- + WT	GOBP_INFLAMMATORY_RESPONSE	3.630E-15	-2.072E+00	538
GO:0002521	Pγ-/- + WT	GOBP_LEUKOCYTE_DIFFERENTIATION	1.930E-08	-1.897E+00	419
GO:1903047	Pγ-/- + WT	GOBP_MITOTIC_CELL_CYCLE_PROCESS	3.075E-01	-1.120E+00	651
GO:0071674	Pγ-/- + WT	GOBP_MONONUCLEAR_CELL_MIGRATION	3.123E-04	-1.873E+00	137
GO:0033865	Pγ-/- + WT	GOBP_NUCLEOSIDE_BISPHOSPHATE_METABOLIC_PROCESS	5.906E-01	-1.013E+00	100
GO:0051130	Pγ-/- + WT	GOBP_POSITIVE_REGULATION_OF_CELLULAR_COMPONENT_ORGANIZATION	4.631E-02	-1.250E+00	822
GO:0008284	Pγ-/- + WT	GOBP_POSITIVE_REGULATION_OF_CELL_POPULATION_PROLIFERATION	1.790E-05	-1.593E+00	642
GO:0010628	Pγ-/- + WT	GOBP_POSITIVE_REGULATION_OF_GENE_EXPRESSION	1.160E-07	-1.638E+00	828
GO:0002684	Pγ-/- + WT	GOBP_POSITIVE_REGULATION_OF_IMMUNE_SYSTEM_PROCESS	8.810E-12	-1.894E+00	616
GO:0051050	Pγ-/- + WT	GOBP_POSITIVE_REGULATION_OF_TRANSPORT	2.262E-04	-1.508E+00	645

GO:0002711	Pγ-/- + WT	GOBP_POSITIVE_REGULATION_OF_T_CELL_MEDIATED_IMMUNITY	1.957E-02	-1.715E+00	47
GO:0043254	Pγ-/- + WT	GOBP_REGULATION_OF_PROTEIN_CONTAINING_COMPLEX_ASSEMBLY	6.176E-01	-9.953E-01	334
GO:0051338	Pγ-/- + WT	GOBP_REGULATION_OF_TRANSFERASE_ACTIVITY	3.909E-03	-1.387E+00	726
GO:0009615	Pγ-/- + WT	GOBP_RESPONSE_TO_VIRUS	1.340E-05	-1.814E+00	307
GO:0042274	Pγ-/- + WT	GOBP_RIBOSOMAL_SMALL_SUBUNIT_BIOGENESIS	1.332E-01	1.362E+00	73
GO:0042255	Pγ-/- + WT	GOBP_RIBOSOME_ASSEMBLY	2.770E-01	1.233E+00	59
GO:0042254	Pγ-/- + WT	GOBP_RIBOSOME_BIOGENESIS	6.477E-01	9.800E-01	298
GO:0042330	Pγ-/- + WT	GOBP_TAXIS	3.010E-10	-1.990E+00	407
GO:0019079	Pγ-/- + WT	GOBP_VIRAL_GENOME_REPLICATION	9.383E-04	-1.827E+00	114

Variant ID (hg38)	Protein Consequence	Database	Sample Size (n)
3-12379738-GC-G	p.Thr41ProfsTer12	All of Us	245400
3-12379750-TG-T	p.Ile45SerfsTer8	Regeneron Genetics Center (RGC) Million Exome	983578
3-12379805-A-AT	p.Lys63GlnfsTer7	1000G	2548
3-12379837-C-CATTT	p.Ser74TyrfsTer24	All of Us	245400
3-12379855-C-G	p.Tyr78Ter	RGC Million Exome	983578
3-12379813-CT-C	p.Phe65SerfsTer33	RGC Million Exome	983578
3-12381372-C-T	p.Gln121*	Framingham Heart Study (FHS)	1637

Table S5

Human variants in PPARG upstream of M135, with columns for Variant ID (hg38), Protein Consequence, Database, and Sample Size (n). Each variant encodes a frameshift (fs) that results in a termination (Ter) or a stop codon (\*), and the protein consequence is relative to ENSP00000287820.6. The first variant, p.Thr41ProfsTer12, encodes a stop codon at amino acid 52 on Exon 1. The second variant, p.Ile45SerfsTer8, encodes a stop codon at amino acid 52. The third variant, p.Lys63GlnfsTer7, encodes a stop codon at amino acid 69. The fourth variant, p.Ser74TyrfsTer24, results in a stop codon at amino acid 97. The fifth variant, p.Tyr78Ter, encodes a stop codon at amino acid 78. The sixth variant, p.Phe65SerfsTer33, encodes a stop codon at amino acid 97. The seventh variant, p.Gln121\*, encodes a stop codon at amino acid 121. All of these occur upstream of p.M135.

**Table S6** Metabolic syndrome severity score (METSS) statistics for carriers of PPARG Pro12Ala (rs1801282) in the UKB. Increasing alleles of Ala are associated with decreasing METSS.

Genotype	n carriers	Median METSS	Mean METSS	Standard Deviation
Pro/Pro	287785	0.0035	0.0087	1.0015
Pro/Ala	75619	-0.0326	-0.0260	0.9947
Ala/Ala	5263	-0.0839	-0.0964	0.9796



**Table S7** Primer sequences for qPCR of PPARgamma target genes in THP-1s and SGBS cells. Related to Figure 1G, 3C, and S1B.

Gene	Forward Primer	Reverse Primer
ADIPOQ	CTGATTCCATACCAGAGGGGCT	GGCCCTTGAGTCGTGGTTT
ANGPTL4	GGCGAGGACACGGCCTAT	AAACCACCAGCCTCCAGAGA
CD11b	GCTTTGGTGGCTTCCTTGTG	CATGACATAAGGTCAAGGCTGT
CD36	TGTCATTGGTGTCTGTCCTGG	TTCTTCGAGGACAACCTTGCTTT
CD68	CTTTGCTGCCATCCTTCACG	CCGAGAATGTCCACTGTGCT
FABP4	ATGGGGGTGTCCTGGTACAT	CTTTCATGACGCATTCCACCA
GAPDH	CATCTTCTTTTGCGTCGCCA	TTAAAAGCAGCCCTGGTGACC
PDK4	GCAGTGGTCCAAGATGCCTT	GTTCAACTGTTGCCCGCATT
PLIN2	CAGTTGATCCACAACCGAGTG	TTCTGGATGATGGGCAGAGC